DELPHI Collaboration

DELPHI 2000-164 PROG 242
09 October, 2000

REMCLU: a package for the Reconstruction of ElectroMagnetic CLUsters at LEP200

F. Cossutti, A. Tonazzo
CERN

F. Mazzucato
INFN and Università degli Studi di Padova

Abstract

Electrons and photons reconstruction and identification is an issue of great importance for many physics analyses at LEP2. The variety of topologies and energy ranges in which they can appear required an improvement of the previous LEP1 pattern recognition. The REMCLU package has been built in order to improve the previous tools for the barrel part of DELPHI, and to provide an efficient general purpose algorithm for the forward part of the detector.

1 Introduction

Electrons and photons reconstruction and identification is an issue of great importance for many physics analyses at LEP2. The pattern recognition tools to handle electromagnetic showers developed at LEP1, ELEPHANT and PXPHOT [1], where thought mostly to deal with electrons and photons in hadronic jets. The main source of energetic isolated electromagnetic showers was Bhabha events, easily selected using simple topological cuts.

The situation at LEP2 is completely different. The number of possible final states has significantly increased, and electrons and photons can show themselves in a large variety of topologies and energy ranges. In this new situation the old pattern recognition was not optimal to handle high energy showers. The situation was particularly unsatisfactory in the forward region due to big size showers developing in the material in front of the FEMC and the poorest performances of the tracking in that region: this caused the LEP1 approach, based essentially on the E/p cut, to be clearly not suitable for objects where it is often difficult to tag a single clean track.

The REMCLU (Reconstruction of ElectroMagnetic CLUsters) package has been developed in order to solve these problems. In the barrel part of the detector it still relies on the ELEPHANT/PXPHOT pattern recognition, using its results for photons and low energy (i.e. < 30 GeV) electrons, and applying a new clustering algorithm for higher energy electrons. In the forward part it implements a new algorithm, based on previous studies on the FEMC pattern recognition and on the new forward tracking [2], exploiting the extension down to 10^o of the Silicon Tracker.

The note is organized in the following way: section 2 describes briefly the updates to the barrel electron/photon search. Section 3 presents a detailed explanation of the new forward search algorithm and of its own performances. Section 4 describes the use of the REMCLU package.

2 Electrons and photons in HPC

2.1 Identification of electrons

Different criteria for electron identification are used in the HPC region for low and high momentum tracks.

First of all, a veto is set on all particles identified as muons. For tracks below 30 GeV, the traditional electron identification algorithm of the ELEPHANT [1] package is used. The algorithm is based on a combination of information from the energy-momentum ratio (E/p), on the dE/dx in the TPC, on the matching of the track to the shower in the z and ϕ directions and on the shower profile. The criteria were developed at LEP1 to discriminate electrons from pions, and are suitable for identification of low energy electrons. Tracks which are tagged at least as "loose" electron by ELEPHANT are considered as electron candidates by REMCLU.

For tracks with momentum higher than 30 GeV, a new, simpler tagging algorithm has been developed to ensure maximal efficiency and to minimize the dependence on the details of the simulation. The photons in a region around the direction of the track are assigned to it. The acceptance for the assignement is of $\pm 2^o$ in the θ direction, while in ϕ it is asymmetric ($-2^o < \Delta(\phi_\gamma - \phi_{electron}) \times \frac{q_{electron}}{|q_{electron}|} < 5^o$) to account for the bending of the track in the magnetic field. The clustered energy is required to be larger than 10 GeV, and its ratio to the track momentum (E/p) must be at least 0.5.

Finally, the energy deposited in the hadron calorimeter in a 5^o cone around the track direction is considered: if it exceeds 10% of the electromagnetic energy (25% near HPC ϕ cracks), the electron is flagged as "loose" by REMCLU.

2.2 Electron energy estimate

The best estimate of the electron energy is obtained from a weighted average of the measured track momentum and of the energy deposited in the HPC. The track momentum is refitted excluding hits in the OD, to minimize the effect of the energy radiated behind the TPC. The energy deposited in the HPC is corrected for non-uniformity effects (cracks) and non-linearity at low energy. The weight given to the energy in the combination depends on the correction factor applied, so that a smaller weight is given to clusters whose energy is corrected by a large amount.

In addition, an error on the best energy estimate is computed for each electron.

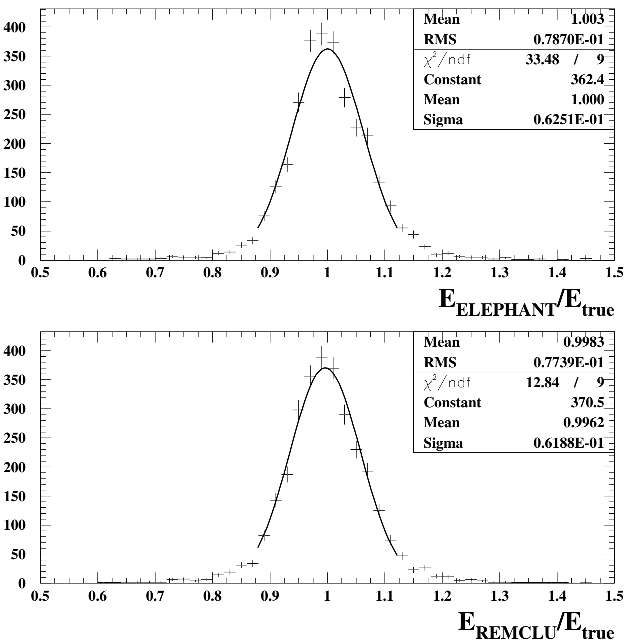

Figure 1: Best estimate of the electron energy in ELEPHANT (upper plot) and REMCLU (lower plot) divided the beam energy. A sample of simulated 45 GeV Bhabha electrons has been used.

In fig. 1 the difference between the best energy estimate of ELEPHANT and REMCLU is shown. A sample of simulated 45 GeV Bhabha electrons has been used. In fig. 2 the fraction of the total cluster energy coming from clusterized secondary PAs is shown: as can be seen the clustering algorithm slightly improves the energy evaluation in about 5% of the cases.

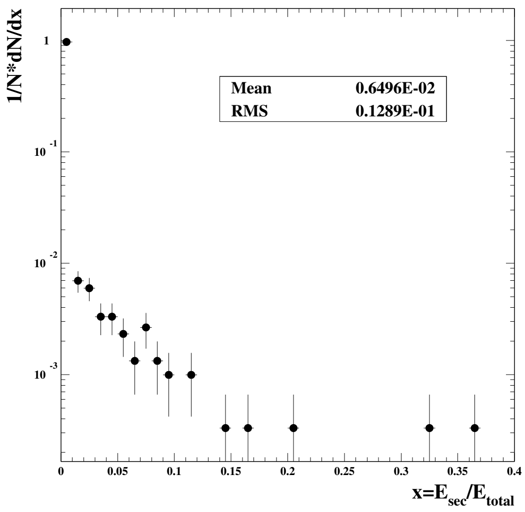

Figure 2: Fraction of the total cluster energy coming from clusterized secondary PAs.

2.3 Treatment of photons

Neutral HPC clusters are considered for photon identification if their energy is at least 500 MeV.

Photon identification relies mainly on the algorithms of the PXPHOT package, based on the longitudinal and transverse development of the shower. For the transverse development, the dispersion of the deposits with respect to the shower direction is considered, and in addition the cluster must not present the clear double-peak structure of $\pi^0 \to \gamma\gamma$ decays. For the longitudinal development, cuts are applied on the shower starting point, on the number of consecutive pad-rows with signal (at least three), and on the radial position of the shower centre of gravity.

Showers with energy below 25 GeV close to a z or ϕ crack are accepted even if they fail the requests on the transverse profile, since the shower shape is less accurately determined near the edge regions of the detector. Such photons are flagged as "loose" by REMCLU. Low energy showers failing longitudinal profile cuts were found to be due to α particles from the lead converter activity in coincidence with electronic noise, and thus are not accepted. Above 25 GeV, the photon close to the cracks is flagged as "loose" even if it fails the cuts on the longitudinal shower development.

3 Electrons and photons in the forward region

3.1 Introduction

The identification of electrons and photons begins inside DELANA [3]: first electromagnetic showers are built inside the calorimeters and tracks are reconstructed with the tracking detectors, then a matching is performed. A detailed description of the reconstruction of electro-magnetic showers in FEMC and STIC can be found respectivly in [5],[6].

In the forward region the efficiency of the whole procedure is degraded, due to the reduced redundancy in the tracking coverage and to the high number of radiation lengths

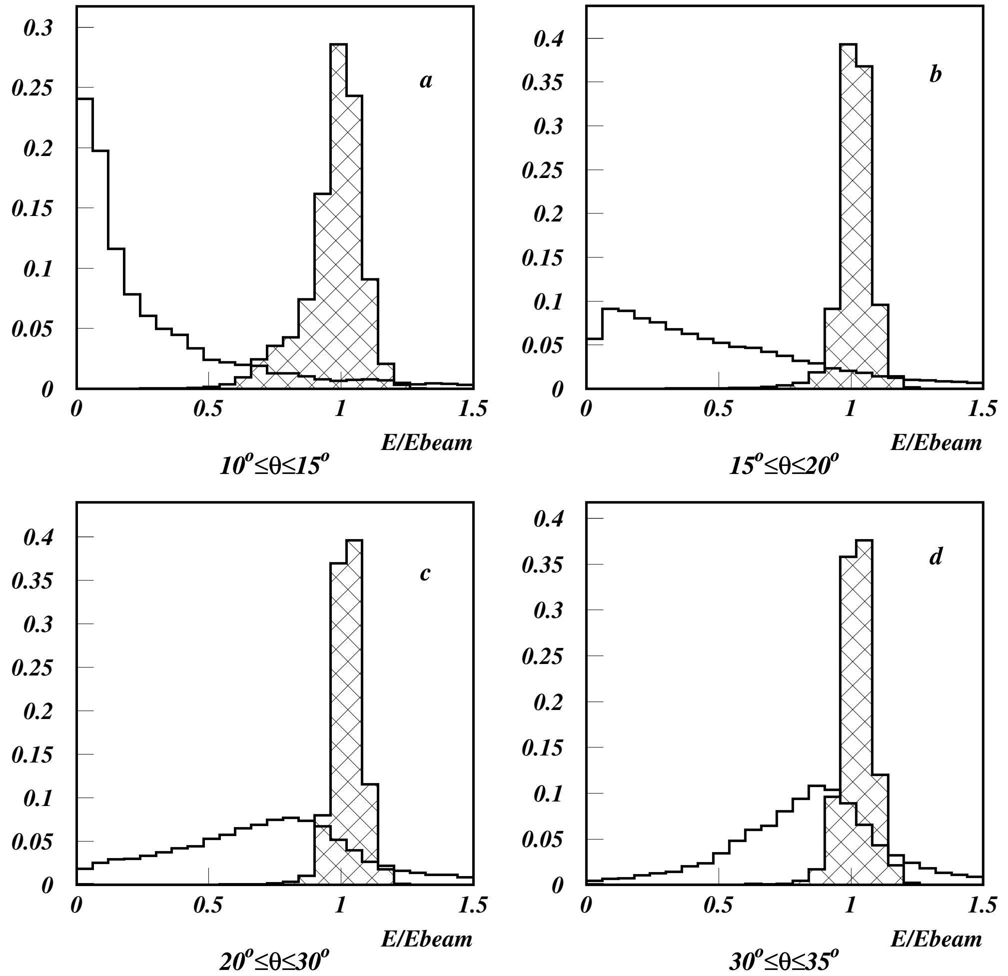

Figure 3: Comparison between the total track momentum (solid) and the total energy in FEMC (hatched) for a Bhabha sample, in different polar ranges: $10^o \leq \theta \leq 15^o$ (a); $15^o \leq \theta \leq 20^o$(b); $20^o \leq \theta \leq 30^o$(c); $30^o \leq \theta \leq 35^o$ (d)

that particles have to pass before reaching the calorimeters. In particular in front of the FEMC there is at least one X_0 of material and in the regions below 13^o or above 32^o more than two X_0. However in the forward region the electron's momentum reconstructed by the tracking devices can be of poorer quality than the energy measured by the FEMC, as can be seen in fig. 3 for a Bhabha sample in different polar ranges. Therefore calorimeters were considered as a starting point for the new identification of electromagnetic showers.

3.2 Algorithm for electron and photon identification in the forward region.

The algorithm developed to reconstruct electrons and photons in the forward region combines information from the calorimetry and the tracking devices to obtain an efficient identification, high purity and the best possible estimate for the energy, direction, and charge of the particle.

The first step is to apply a re-clustering to FEMC showers, section 3.2.2, so as to recover the energy degradation due to early showering in the material in front of the calorimeter. Then the matching with tracking is performed to achieve the particle identification, section 3.2.3. For tagged electrons the direction measured by the calorimeter is replaced by that of the associated track, so as to take into account the bending due to the magnetic field, section 3.2.4. Finally the isolation of the particle is discussed, sec 3.2.6.

Former studies [4] showed that one cannot neglect the probability of rejecting a good and possibly energetic electro-magnetic shower because it was wrongly associated at DELANA level to a badly measured or very soft track, which is skipped by the standard DELPHI track selection. To be independent from any pre-selection all the charged and neutral particles reconstructed at DELANA level have been considered in this analysis.

In the following the θ dependence of several quantities is studied. Unless otherwise stated, both end-caps are treated together and for the one placed at θ greater 90^o the complementary angle ($180^o - \theta$) is considered so that the FEMC polar range is between 10^o and 36^o.

All the studies have been carried on with both data and Montecarlo samples.

3.2.1 Data samples

In this section the selection criteria for the different samples used in the studies are summarized. Unless otherwise stated all the samples correspond to a centre-of-mass energy of 200 GeV.

- Bhabha (type 1).
  At least two electro-magnetic clusters in the FEMC having more than half the beam energy each and collinear within 2^o.

- Bhabha (type 2).
  At least two electro-magnetic clusters in the FEMC having more than half the beam energy each and collinear within 5^o but with at least 1^o of acoplanarity so as to reject the QED process $e^+e^- \rightarrow \gamma\gamma$.

- Bhabha (type 3).
  Two electro-magnetic clusters in the FEMC identified as electrons (by REMCLU, this selection is used only to study the angle reconstruction). No other electro-magnetic cluster. Each of the electron having more than 95% of the beam energy.

- Bhabha (type 4).
  At least two electro-magnetic clusters in the FEMC having more than half the beam energy each and collinear within 5^o. If other electro-magnetic showers are present they must be outside a 20^o cone around each of the main clusters in order to assure the isolation.

- Hadronic radiative return to the Z.
  They have a very clean signature if the radiative γ falls in the acceptance of the detector because its energy peaks at $E^*_\gamma = (s - m_Z^2)/(2\sqrt{s})$. Moreover they are three-body final states therefore they lay in a plane and it is possible to compute the energies from the measured directions. Events are then selected if they were planar

within 1^o, they had an energetic photon with $(E^*_\gamma - 5)\text{GeV} < E_\gamma < (E^*_\gamma + 5)\text{GeV}$ seen by the detector and the photon energy computed from the direction was no more than 20% away from the measured energy.

3.2.2 Clustering in the calorimeter

A sample of Bhabhas of type 1 can be used to study the re-clustering scheme in the FEMC. In order to reject muons, showers are considered only if they have energy above 3 GeV and $E_i^{em}/(E_i^{em} + E_i^{ha})$ above 0.9 where E_i^{em} is the electro-magnetic energy of shower i and E_i^{ha} its associated hadronic energy.

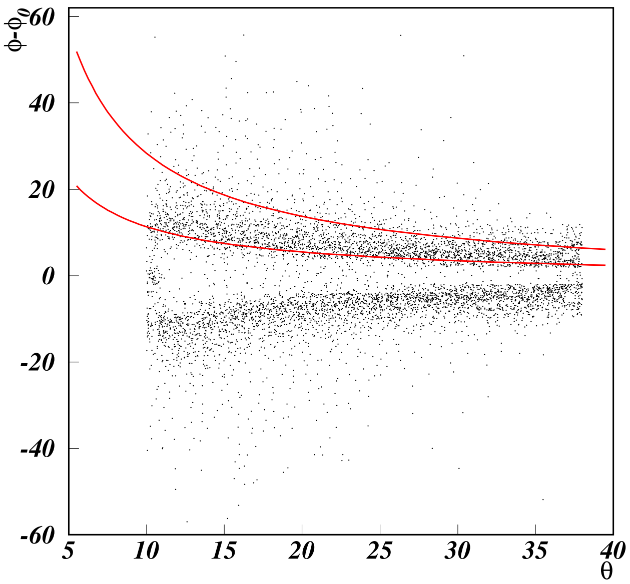

Figure 4: $\Delta\phi$ spread of an electromagnetic cascade in FEMC.

Fig.4 shows the distribution of the distance in ϕ between the most energetic shower in the end-cap and the secondaries, as a function of theta. The number of entries in each y-bin is weighted by the total number of events in the corresponding theta range. The superimposed solid lines are parametrised by:

$$\Delta\phi = |\phi - \phi_0| = 2^o/tg(\theta) \quad (lower) \tag{1}$$
$$\Delta\phi = |\phi - \phi_0| = 5^o/tg(\theta) \quad (upper) \tag{2}$$

where ϕ_0 is the coordinate of the most energetic shower. The physical reason for the $\Delta\phi$ spread is that charged secondaries particles produced during the showering before the FEMC are bent, due to the magnetic field, in the (R,ϕ) plane. The behaviour of the $\Delta\phi$ as a function of θ distribution can be easily explained in terms of the FEMC geometry. The ϕ distance between two showers whose central glasses are separated by N counters (see the picture 5) can be computed as:

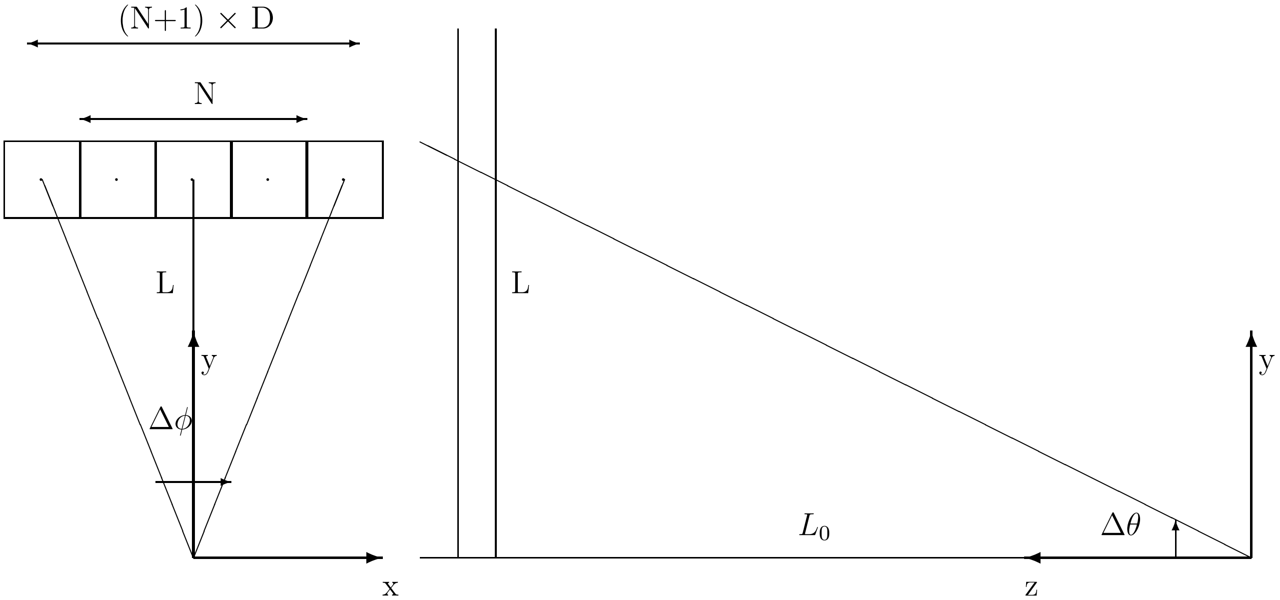

Figure 5: Geometrical relationship between the FEMC glasses geometry and the secondary showers spread $\Delta\phi$.

$$\Delta\phi = arctg\left(\frac{(N+1)\times D}{L}\right) = arctg\left(\frac{(N+1)\times D}{L_0 \times tg(\theta)}\right) \tag{3}$$

where N is the number of counters between the central glasses, D = 5 cm is the dimension of one counter, L_0= 284 cm is the mean distance of each FEMC end-cap from the interaction region. In the approximation of small $\Delta\phi$, this becomes:

$$\Delta\phi \simeq \frac{N+1}{tg(\theta)} \times \frac{D}{L_0} \tag{4}$$

and expressing the angles in degrees:

$$\Delta\phi \simeq \frac{N+1}{tg(\theta)} \tag{5}$$

It is now easy to understand that the depletion around $\Delta\phi \simeq 0$ is due to the basic clustering at DELANA level which was described in [5]: the minimum distance to reconstruct two separate showers corresponds to N=2 glasses. Most of the secondaries are within 5 glasses from the most energetic one.

Fig. 6 shows the distribution of the polar distance between the most energetic shower in the end-cap and the secondaries, as a function of theta. The $\Delta\theta$ distribution is flat and the spread is much reduced compared to $\Delta\phi$ because there is no bending due to the magnetic field in θ. The solid lines correspond to $\Delta\theta = \pm 3^o$

As a first step in the clustering procedure, all secondary showers which are contained in a volume around the most energetic, defined by $|\Delta\theta| < 3^o$ and $|\Delta\phi| < 5^o/tg(\theta)$ are clustered together with a recursive procedure, starting from the most energetic. Each time a new shower is added the energy and direction of the cluster are recomputed. The new

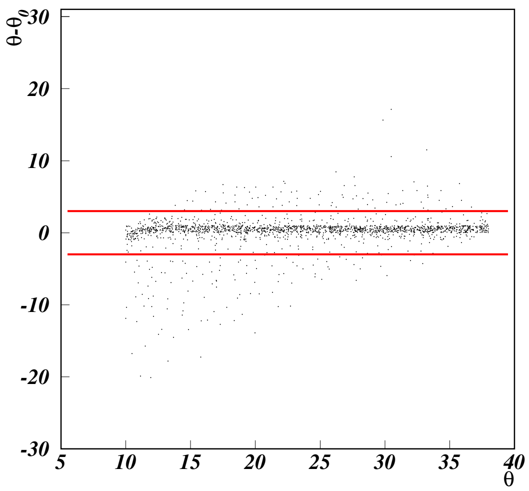

Figure 6: θ spread of an electromagnetic cascade in FEMC.

energy of the cluster is obtained as the sum of the energies: $E^{cluster}_{new} = E^{cluster} + E^{shower}$. The new direction is evaluated with a center-of-gravity technique:

$$Xi^{cluster}_{new} = \frac{Xi^{cluster} \times E^{cluster} + Xi^{shower} \times E^{shower}}{E^{cluster} + E^{shower}} \tag{6}$$

where i=1,2,3 and Xi are cartesian coordinate.

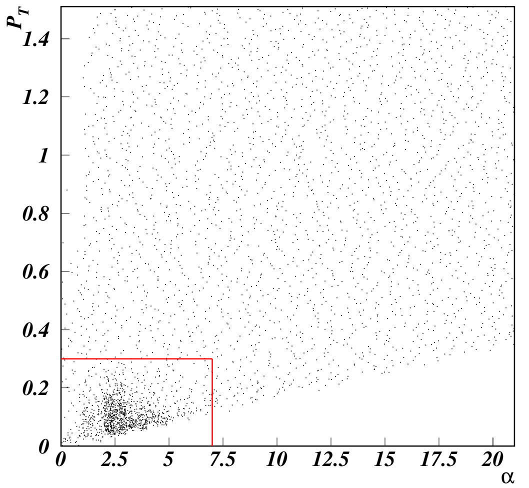

Figure 7: Distribution of the transverse momentum of secondary showers with respect to the main cluster, as a function of their angular distance α

For secondary showers which are not clustered according to these criteria the transverse momentum p_t with respect to the main cluster is computed. Fig. 7 shows the scatter plot of p_t versus the angular distance between the main cluster and the secondary, unassociated, shower. The bulk of secondary showers are contained in a 7^o cone around the cluster and have $p_t < 0.3\,\text{GeV}$. As a second step all these showers are reclustered as well with the same technique as before.

For clusters at the edges of FEMC part of the energy is lost because not all the secondaries are contained in the calorimeter. However, at low polar angle some of the energy which escapes the FEMC detection can be recovered using electro-magnetic clusters reconstructed by the STIC. The clustering procedure is analogous to that used for FEMC showers.

Using this re-clustering it is possible to obtain a better energy resolution, as shown in fig 8, for the Bhabha in the real data sample at 200 GeV. The upper plot shows the sum of the energies of the two most energetic showers in FEMC reconstructed at DELANA level, while in the lower plot the two most energetic clusters built with the algorithm described are considered. The resolution improves from 5.3 GeV to 4.7 GeV and the tail at $E/E_{beam} \ll 1$ is reduced. Moreover if one counts the number of clusters instead of the number of charged and neutral particles in the event, a correct multiplicity can be recovered, as shown in fig 9, where the total number of FEMC clusters, of charged tracks and neutral particles are shown for Bhabha events.

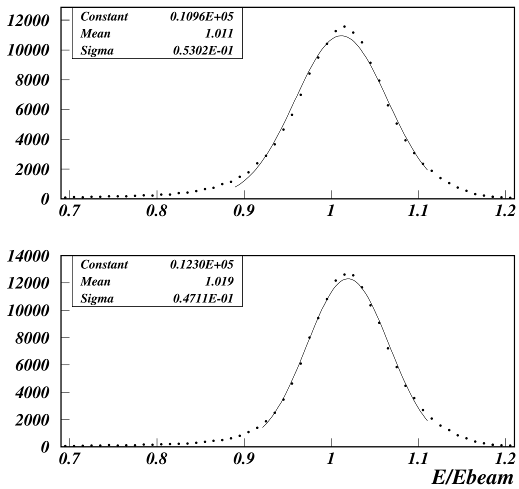

Figure 8: Real Bhabha energy resolution at 200 GeV.

3.2.3 Identification

Electrons and photons can be separated by checking if there is a charged track associated to the cluster reconstructed in the FEMC. Nevertheless, due to the high probability of showering before the calorimeter it is likely that some tracks, generated by secondary particles, can be found also for photons. A way out is to consider for the electron identification only those tracks which start from the innermost detectors, because they have a lower probability of being generated by a conversion. For example a study [7] carried on a $e^+e^- \rightarrow \gamma\gamma$ sample, with one of the γ converted, has shown that the probability of

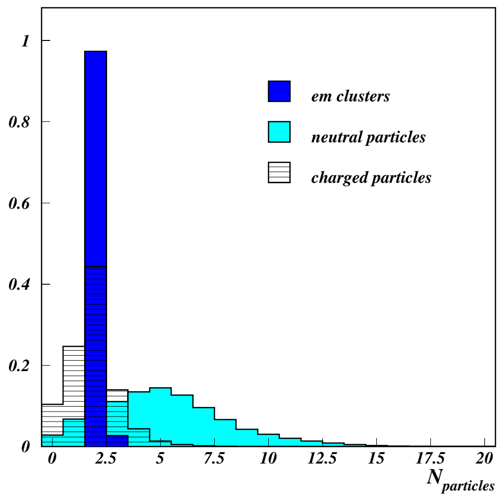

Figure 9: Bhabha multiplicity using clusters, charged particles or neutral particles.

having a γ conversion in the beam pipe which generates hits in the vertex detector is only 0.6%.

To associate a track to a FEMC cluster, the position and direction of the cluster are extrapolated to the first measured point of the track. The trajectory goes from the FEMC to the primary vertex if it is reconstructed, to the beam spot, if not. All charge hypotheses (q=+1,0,-1) are considered. In the charged hypothesis the extrapolation is performed along an helicoidal path which is fully determined by the momentum of the particle, its charge and the magnetic field. The energy measured in the FEMC is used as momentum estimate for the extrapolation. In the neutral hypothesis the extrapolation is performed along a straight line throught the two fixed points.

The aim is to recover the information from tracks which were not yet part of the cluster (e.g. they had no electro-magnetic energy associated). The association criteria are defined and optimised using Bhabhas to study the efficiency and photons from hadronic radiative returns to the Z to monitor the fake associations. First the geometrical compatibility is checked: the distance in the (R,ϕ) plane between the first measured point of the track and the extrapolated position of the cluster at the corresponding z coordinate have to be less than 10^o. Then the momentum compatibility is checked: the directions of the momentum extrapolated at the first measured point for the cluster and the track have to be compatibile within 3^o.

Once all the tracks belonging to a cluster have been defined the identification is performed taking into account the number and type of tracks associated and the geometry of the tracking devices. The following classes have been defined:

- tight electrons: one and only one associated track starting from VD-VFT and no more than one TPC+ID track;
- loose electrons: no VD-VFT tracks, one and only one associated ID+TPC track or, if the polar angle is below 20^o, one and only one associated ID+FCH track;
- tight photons: the cluster is above 11^o and has no associated VD-VFT or TPC+ID tracks. If the cluster is below 20^o it is required to have also no associated ID+FCH tracks and if it is below 15^o no associated FCH tracks;

- loose photons: the cluster is above 11^o there are two TPC+ID tracks associated or there are no associated VD-VFT, TPC+ID and, if below 20^o, ID+FCH tracks.

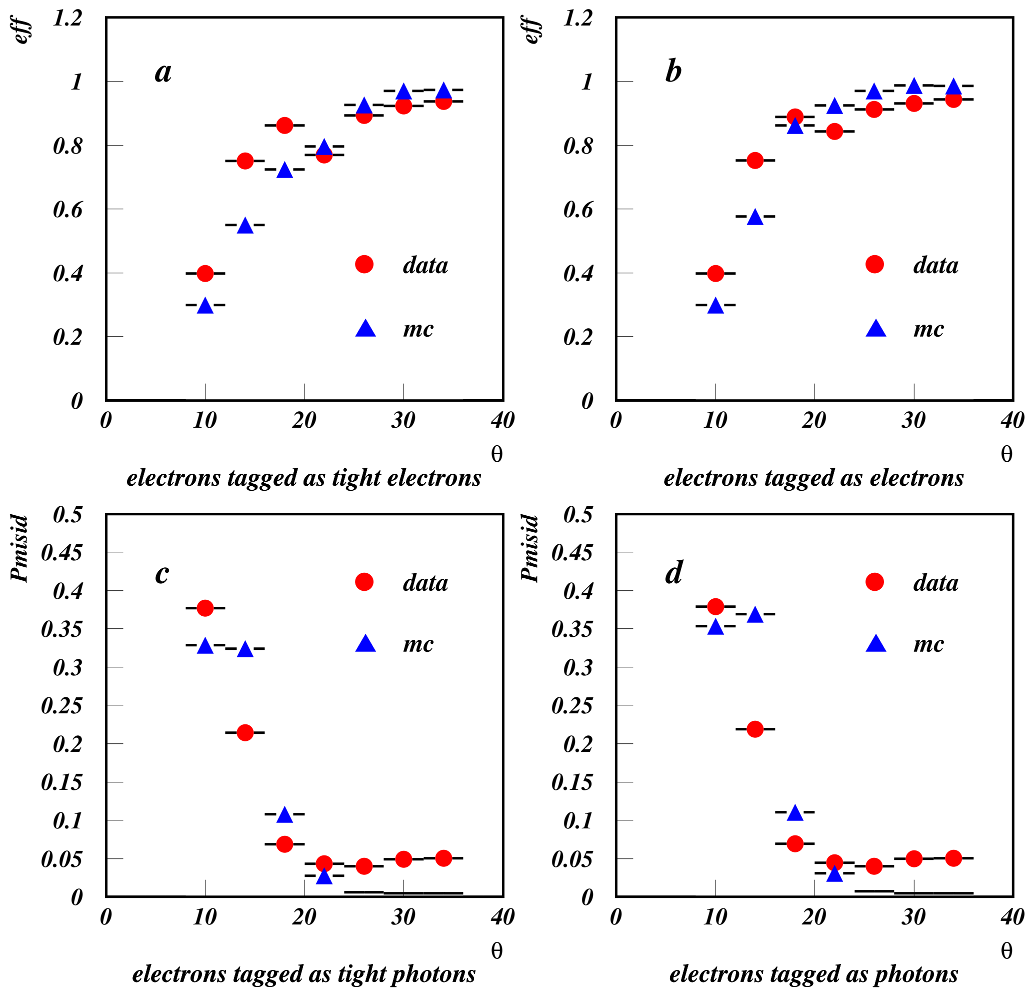

Figure 10: Tagging efficiencies and misidentification probability

The clusters which do not fall in any of these cathegories are classified as 'unknown'. For thight photons below 15^o the requirement of having no FCH tracks associated has been added to decrease the electron contamination: without this requirment more than 50% of the electrons below 15^o would have been tagged as tight photons. If for both charged hypothesis a candidate track is found the one which has $E_{cluster}/p_{track}$ closer to one is considered.

Fig. 10 shows the electron identification efficiency and misidentification probability as a function of the polar angle for data (dots) and Montecarlo (triangles) which was computed using Bhabha of type 2 to obtain an electron sample. Fig. 10 (a) shows the tight electron identification efficiency. In the VFT region the identification efficiency

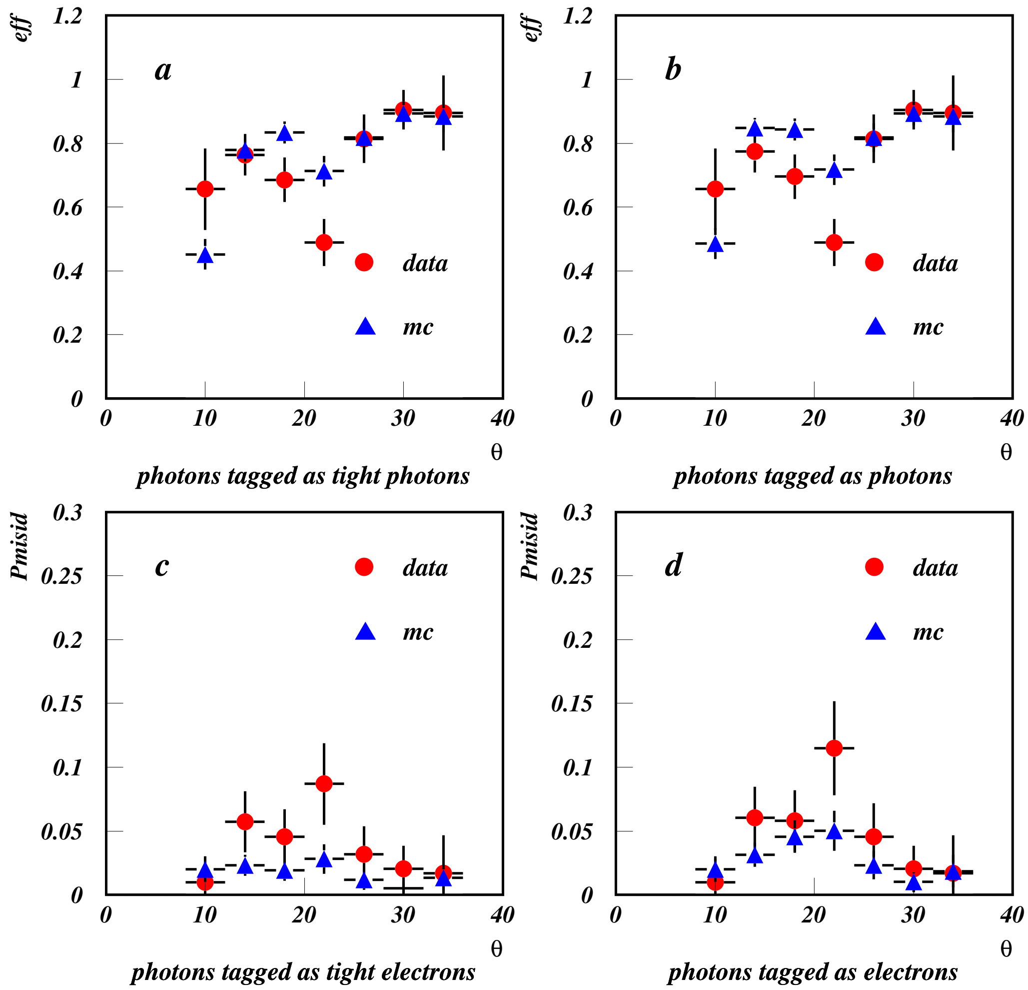

Figure 11: Tagging efficiencies and misidentification percentages

is higher for data than for the simulation, and it increases with the polar angle from 30% to 80%. In the VD region the performances on data and simulation are similar and the efficiency is essentially greater than 80%. Focusing on the data sample only, one can notice that between 18^o and 24^o,the performances are degraded: the electrons identification efficiency decreases from more than 80% to about 75%. This corresponds to the transition between the VFT and the VD regions. In fact at 18^o the Ministrip layer of the VFT ends and only two silicon planes (pixels1 and pixels2) can be used to reconstruct the track up to 24^o where the closer layer of the VD comes into play and the particles cross 3 silicon layers again. Moreover around 20^o the pixel2 layer of the VFT finishes and the inner layer of the VD begins. On top of this the sizable amount of material at the end of the VD can play a role. Fig. 10 (b) shows the total (tight+loose) electron identification efficiency. It should be noticed that in the polar region around $15^o - 25^o$ the loose tag allows to improve significantly the efficiency: 5-10% in the data and up to 15% in the Montecarlo. The fraction of electron misidentified as tight photons is shown in fig. 10 (c) and it is again very dependent on the polar angle. Above 15^o the misidentification probability il always lower than 10% and above 20^o it is of the order of 5% in the data and less for the simulation. Fig. 10 (d) shows the total misidentification probability (tight+loose photons). Considering loose photons, there is a slight increase in the misidentification at low polar angle (below 15^o).

Fig. 11 shows the photon identification efficiency and misidentification probability as a function of the polar angle for data (dots) and Montecarlo (triangles) which were studied with hadronic radiative return to the Z having the photon seen in the detector to obtain a photon sample. Fig. 11 (a) shows the tight photon identification efficiency. The efficiency ranges basically from 60% to 90%. Fig. 11 (b) shows the total (tight+loose) photon identification efficiency. In the polar region around $10^o - 20^o$ the loose tag allows to improve the efficiency: of about 5% in the data and up to 10% in the simulation. The percentage of photons misidentified as tight electrons is shown in fig. 11 (c). It is around 5% over the whole theta range, a few percent higher in the data than in the simulation. Fig. 11 (d) shows the total misidentification probability (tight+loose electrons) is between 5-10%. Considering loose electrons, there is a slight increase in the misidentification between $15^o - 25^o$ of few percent. Bhabha and $\gamma\gamma$ (QED) Montecarlo in which a particle was not correctly classified by the algorithm have been studied using the event display. It was found that this is typically related either to a verly early showering in the detector or to inefficiencies in the pattern recognition. Fig. 22-25 show the display of some Bhabha Montecarlo events in which one of the electrons is not classified as tight electron. Fig. 26-28 show the display of some Montecarlo $\gamma\gamma(QED)$ events in which the photon is not classified as tight photon.

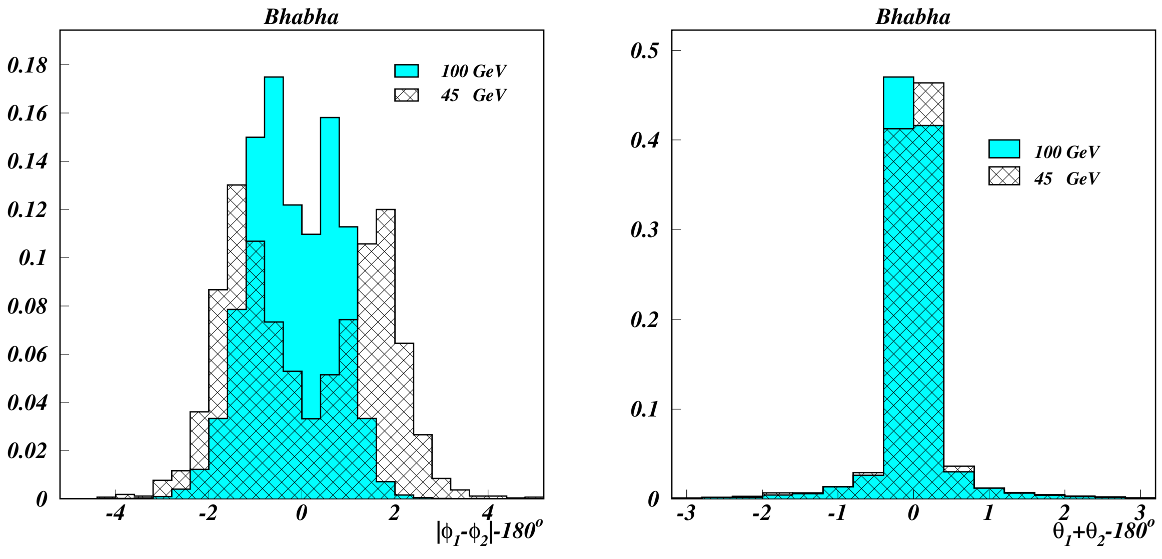

Figure 12: Left:Acoplanarity between two FEMC clusters for Bhabha at 100 GeV and 45 GeV. The bending of the trajectories in the (R,ϕ) plane is due to the magnetic field. Right: Difference in the polar coordinate between two FEMC clusters for Bhabha at 100 GeV and 45 GeV.

These results have been obtained with the new DELPHI tracking algorithm which was used from the 1999 data-taking on. The most important difference between the new algorithm and the old one is the improvement in the pattern recognition in the VFT region. A comparison between the identification performances obtained with the two algorithms was performed. An overall improvement is obtained with the new tracking, but of course the biggest gain is obtain below 18^o, in the VFT region: the percentage of tagged electrons grows from 10-15% to more than 40%.

3.2.4 Direction

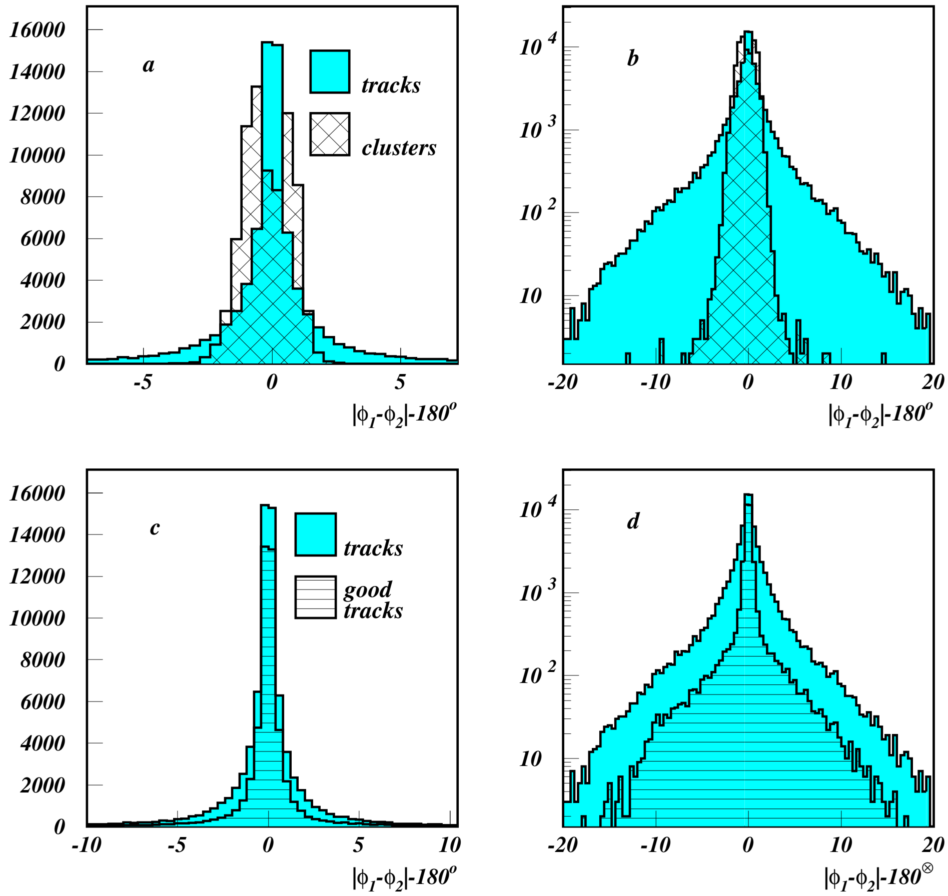

Figure 13: Acoplanarity in the (R,ϕ) plane for Bhabha events in linear (left) and logarithmic (right) scale. The acoplanarity is computed using the direction measured by the calorimeter (hatched) or by all the tracks (shaded) or by the subsample of tracks classified as good (lines)

For photons the direction reconstructed with the FEMC is correct, whereas electrons are bent by the magnetic field in the (R,ϕ) plane. This effect can be studied using Bhabha of type 3 and it is not negligible, even for high energy electrons, as for example Bhabha at 100 GeV (high energy run) or at 45 GeV (Z run), as can be seen in fig. 12 which shows the acoplanarity $|\phi_1 - \phi_2| - 180^o$ of Bhabha events, where ϕ_i is the coordinate of cluster i measured by the FEMC.

In absence of magnetic field the distributions would be peaked at zero. Of course the lowest is the electron's momentum, the more pronounced is the bending and thus biggest the ϕ shift. It should be noted that the bending of both electrons contributes to the total shift, which is of the order of 0.7^o for electrons of 100 GeV and 1.5^o for electrons of 45 GeV. In θ no bending is observable, as can be seen in fig. 12, as expected.

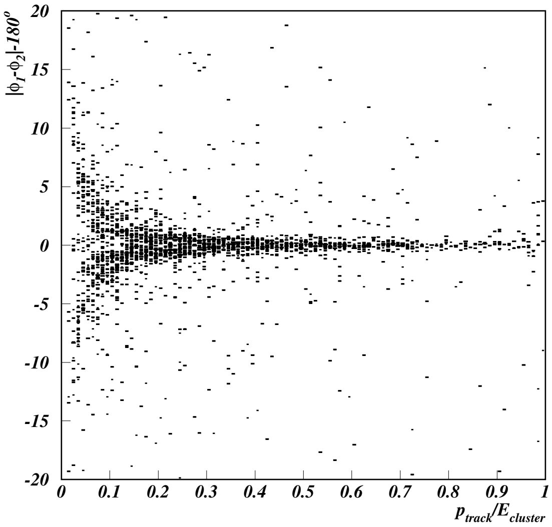

Figure 14: Acoplanarity of Bhabhas compute with the track direction as a function of $p_{track}/E_{cluster}$

The tracking information can be used to improve the direction measurement of the electrons. In this sample both clusters are identified as electrons, therefore one can compare the acoplanarity in the (R,ϕ) plane measured with the calorimeter with that measured using the associated tracks. Results are displayed in the upper plots of fig. 13 in linear and logarithmic scale. It is clear that the use of the direction measured with the tracks corrects for the bending effect, nevertheless some undesired tails appear in around 20 % of the cases. This is due to badly measured tracks, giving a wrong direction information. It is possible to correct this effect defining a subsample of “good tracks”, which satisfy some quality criteria, defined in the following. The acoplanarity has been studied as a function of the impact parameter, the error on the ϕ, the $p_{track}/E_{cluster}$ and the polar dependence. Fig. 14 shows for example the dependence of the acoplanarity on the $p_{track}/E_{cluster}$.

It was decided to define as “good” tracks those either above 25^o or above 11^o and having an $p_{track}/E_{cluster} \geq 0.15$ and an error on ϕ less than 0.5^o. The lower plots in fig. 13 show the comparison between the acoplanarity computed with all tracks and with the subsample of the “good” ones only, in linear and logarithmic scale. With this requirement about 80-90% of the events in the tails are rejected, while only 10% of the events in the peak at zero are cut. For the polar angle a similar study has been carried on, and the results are shown in fig. 15. Using the direction measured by the tracks, the θ resolution slightly improves with respect to that obtained with the clusters and no tails are observed.

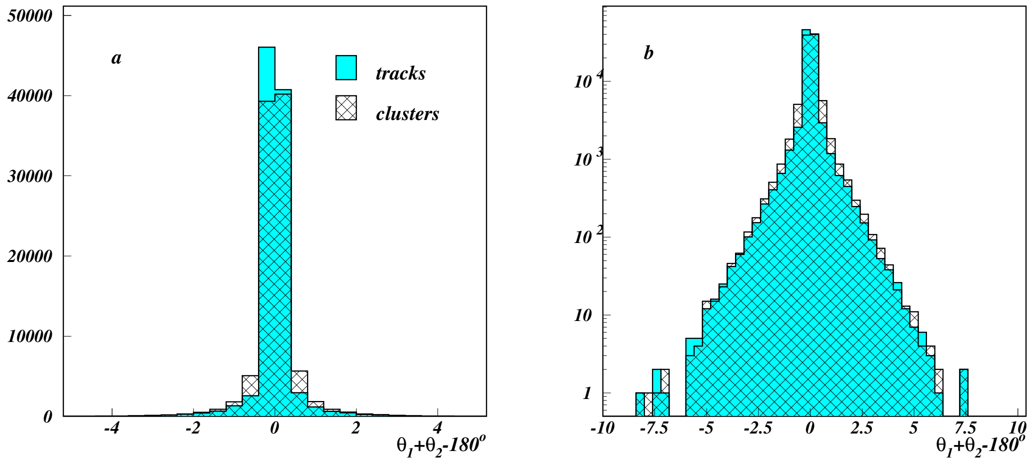

Figure 15: Acolinearity in θ for Bhabha events in linear (left) and logarithmic (right) scale. The acoplanarity is computed using the direction measured by the calorimeter (hatched) or by all the tracks (shaded)

3.2.5 Energy resolution

The FEMC energy resolution, was measured during the test beams to be:

$$\frac{\sigma_E}{E} = \sqrt{\left(\frac{0.05}{\sqrt{E}} + 0.355\right)^2 + \frac{0.2^2}{E}} \tag{7}$$

The stochastic term, $0.05/\sqrt{E}$ is typical of lead glass calorimeters. However, inside DELPHI the energy resolution is degraded due to the pre-showering of the electrons/photons in the material before the FEMC.

A sample of Bhabha events (type 1) at 200 GeV can be used to estimate the polar dependence of both the energy resolution and the ratio E_{mea}/E_{true} between the measured energy of the cluster and the beam energy. The results are shown in fig. 16 for both data (squares) and simulation (dots). Below 15^o and above 32^o the performances are degraded in both samples. This is mainly due to two causes: in these regions the amount of material before the FEMC is bigger; at the edges of the FEMC part of the energy can be lost because the showers are not fully contained.

Real data and Montecarlo have a different dependence of the resolution on the polar angle. In the central region the energy resolution is found to be around 4-4.5% for data and 5-5.5% for Montecarlo. At the FEMC edges the discrepancy increases: for Montecarlo the resolution is less than 8% while for data it can reach 12%. This effect is mainly due to the difficulty in simulating correctly the material in front of the FEMC.

The energy resolution depends on the energy range considered. The former study has been repeated using Bhabhas at the Z peak (91 GeV), again for both real data collected during the year and for Montecarlo. The general behaviour is similar to what observed at high energy. If one compares the two energies, fig. 17, at $\sqrt{s} = 91$ GeV the resolution is always about 3% worst. The ratio between measured energy and beam energy becomes smaller at low polar angle because the spread of the cluster is bigger and the re-clustering is less effective.

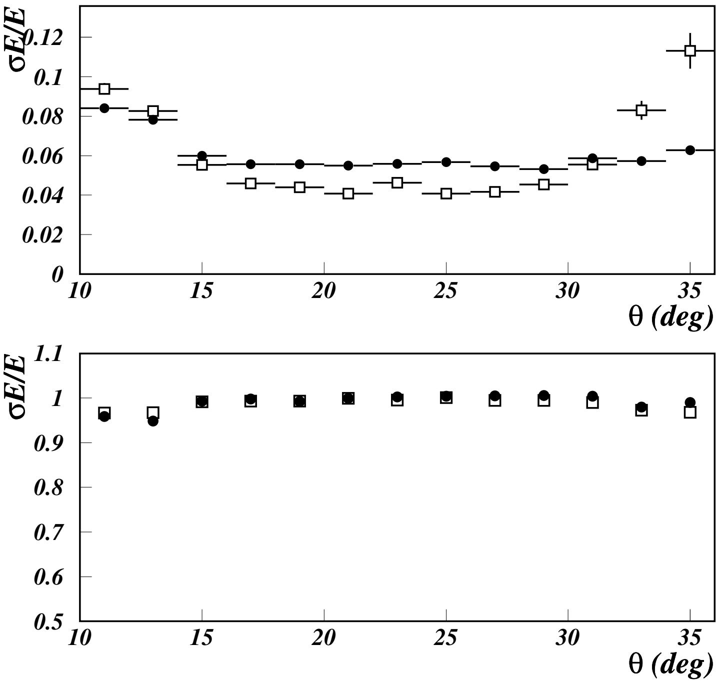

Figure 16: Polar dependence of the ratio between the measured and the beam energy (bottom) and of the energy resolution (top), using a Bhabha sample at 200 GeV, for data (squares) and Montecarlo (dots).

Up to now the energy resolution has been computed with non radiative Bhabha which have a fixed energy equal to half the centre-of mass energy. However the energy resolution can be estimated on the whole range from zero up to the beam energy using a radiative Bhabha sample $e^+e^-\gamma$ with both the electrons and the photon detected. Assuming no further radiation is emitted, these events are kinematically over-constrained by the measurement of the particles directions and by the centre of mass energy $\sqrt{s}$. Thus, neglecting the electron mass, the "true" energies of the particles can be derived with the formula:

$$E_1^{true} = \sqrt{s}\frac{sin(\delta_{23})}{den}; E_2^{true} = \sqrt{s}\frac{sin(\delta_{13})}{den}; E_3^{true} = \sqrt{s}\frac{sin(\delta_{12})}{den}; \tag{8}$$

where E_i is the energy of the cluster i, δ_{jk} is the angular distance between the particles j and k, and $den = sin(\delta_{23}) + sin(\delta_{13}) + sin(\delta_{12})$.

Particles are numbered in order of decreasing energy. The events used to compute the resolution had to satisfy the following requirements:

1. number of electro-magnetic cluster = 3;
2. $E_1 > 30\%\sqrt{s}$; $E_2 > 25\%\sqrt{s}$; $E_3 > 5\,\mathrm{GeV}$;
3. at least one of the particles inside the FEMC acceptance;

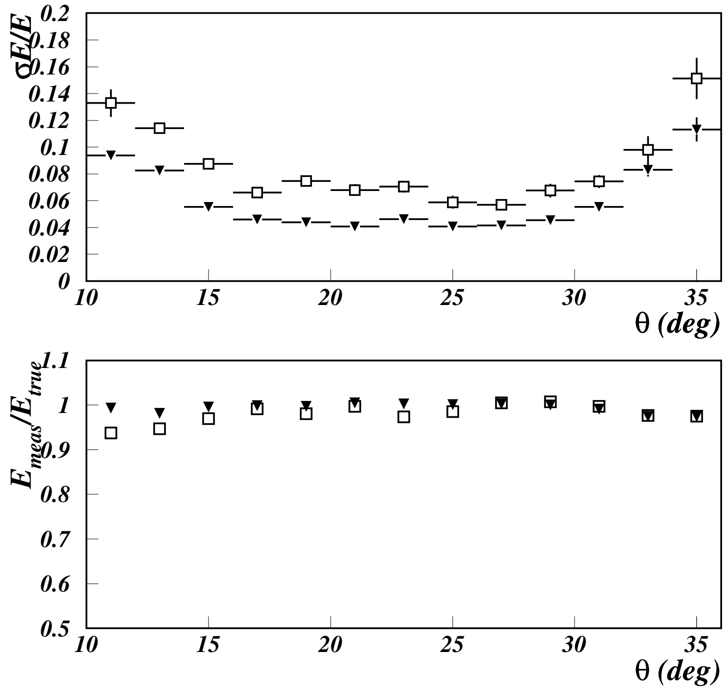

Figure 17: Polar dependence of the ratio between the measured and the beam energy (bottom) and of the energy resolution (top), using a Bhabha samples at $\sqrt{s} = 91$ GeV (squares) and $\sqrt{s} = 200$ GeV (triangles) for real data.

4. $|\Delta| = |\delta_{23} + \delta_{13} + \delta_{12} - 360^o| < 1^o$; $|a| = |arcsin(\vec{u_2} \bullet (\vec{u_1} \times \vec{u_3}))| < 1^o$;
5. $|\delta_{12} - 180^o| > 5^o$; $min(|\theta_1 - \theta_3|, |\theta_2 - \theta_3|) > 2^o$
6. 2 electrons and 1 photon identified;

where $\vec{u_i}$ gives the direction of cluster i. The first three requests select the topology. The fourth criteria guarantees that the three particles lay in a plane, as foreseen for a three body event. This limits the amount of undetected radiation. The fifth requirement has been added to reject clusters which could come from early showering of one of the electrons before the calorimeter. The two electrons must be identified and their direction must be computed with the tracking information. In this way the computation of the true energy from the measured directions is not biased by the bending of the trajectories.

Again both a real data and a Montecarlo sample were considered. The plots on the upper left corner of figures 19 and 18 show, respectively for the data and the simulation, the linearity between the measured and true energy of the FEMC clusters selected over the whole energy range.

The energy resolution depends, as pointed out at the beginning of the section, on the polar angle so three θ ranges have been considered separately: $10^o < \theta < 15^o$, $15^o < \theta < 32^o$, $32^o < \theta < 36^o$. In all angular regions, five bins of energy were considered, of 20 GeV width each and centred at 10, 30, 50, 70, 90 GeV , so as to cover the whole spectrum.

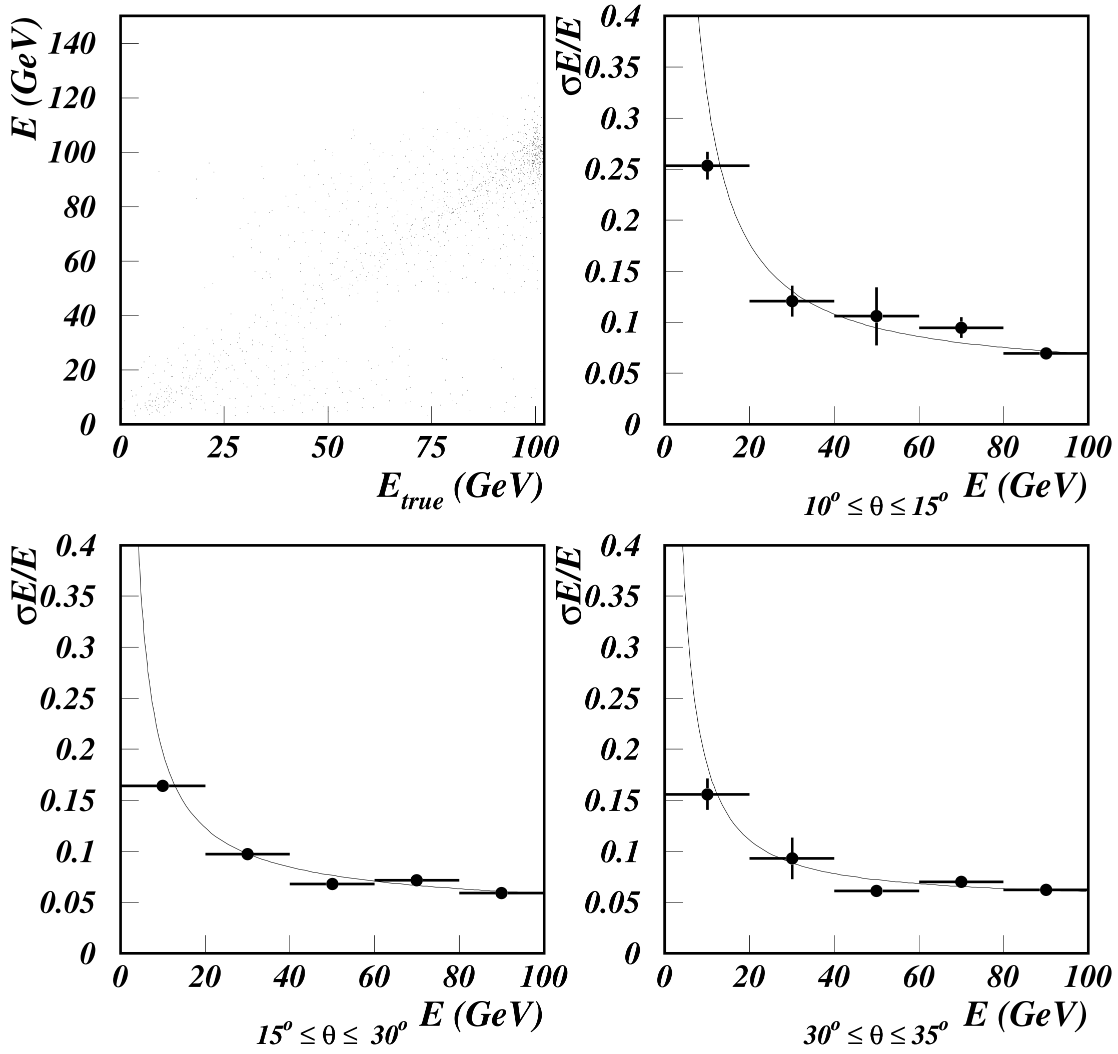

Figure 18: Montecarlo events. Upper left: linearity between the measured and true energy of electro-magnetic clusters in FEMC. The other three plot show for different polar ranges the dependence of the energy resolution on the measured energy.

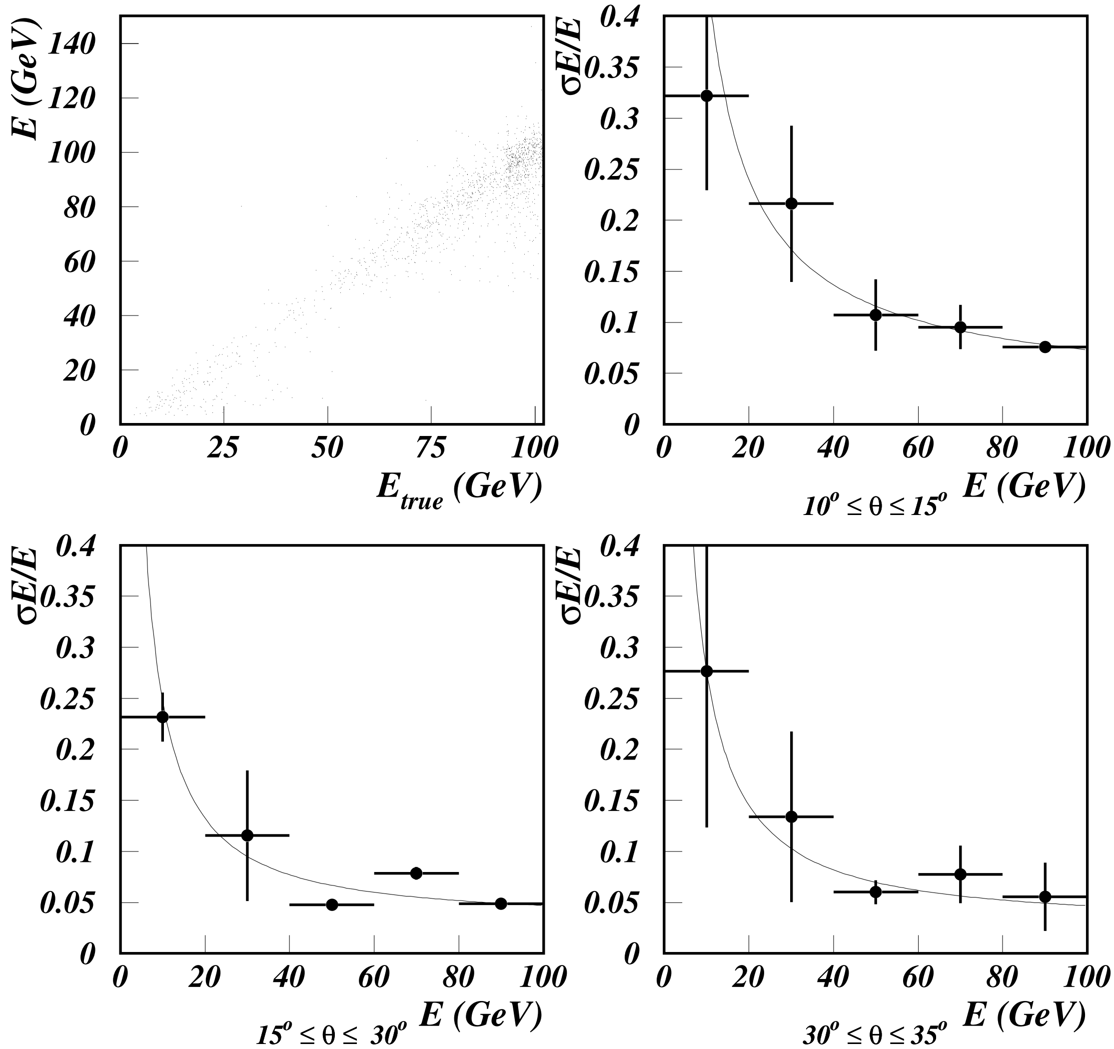

Figure 19: Real data events. Upper left: linearity between the measured and true energy of electro-magnetic clusters in FEMC. The other three plot show for different polar ranges the dependence of the energy resolution on the measured energy.

In each bin the spread $E_{mea} - E_{true}$ of the measured energy around the true energy was computed. The energy resolution σ_E was then estimated with a Gaussian fit to this distribution. The energy distribution of the events is not flat over the bin so the resolution computed was referred to the mean energy measured in that bin, and not to the centre of the bin. The dependence of the resolution on the energy is shown in fig 19 for data and in fig. 18 for the Montecarlo, in the different polar ranges.

For the simulated Bhabha sample, above 40 GeV the resolution is rather flat around 5% in the central region and 7-8% at the border regions.

In real data the resolution ranges from 4.5% at 90 GeV in the central region to more than 30 % at low energies in the border region.

The solid line corresponds to a fit with the usual formula:

$$\frac{\sigma_E}{E} = \sqrt{\left(\frac{A}{\sqrt{E}} + B\right)^2 + \frac{0.2^2}{E}} \tag{9}$$

The values obtained for the A and B parameters of the fit are displayed in table 3.2.5 It is worth mentioning that, as expected, the effect of the material, which causes early showering, affects the stochastic parameter A, which is found to be much worst than in the test beam value.

		$10^o < \theta < 15^o$	$15^o < \theta < 32^o$	$32^o < \theta < 35^o$
DATA	A	0.299	0.131	0.152
	B	0.050	0.040	0.045
MC	A	0.293	0.137	0.154
	B	0.051	0.048	0.050

Table 1: Coefficients of the energy resolution parametrisation 9 in different polar angle ranges.

In the polar region above 32^o the energy resolution for real data is degraded. On the contrary the tracking performances are better in this region than at lower polar angles. A study was thus performed to understand if the tracking information could be used to improve the energy resolution. Fig.20 shows the energy measured and the resolution achieved with the FEMC (triangles) or the tracking (squares) in the polar range above 20^o for Bhabha at $\sqrt{s} = 91$ GeV. A similar study has been performed ad $\sqrt{s} = 200$ GeV.

The energy measured with the FEMC is generally better except at the very edge of the FEMC (polar range $34^o - 36^o$) for not too high energies. The tracking resolution does not depend on the momentum (down to the GeV scale) and for polar angles above 25^o it is rather flat around 15%. The FEMC energy resolution in this polar range is parametrised with eq 9. Below the energy at which the two resolution functions cross the tracking determination of the energy is used, while above the calorimetric measurement is considered.

3.2.6 Isolation

Almost all the studies, described up to now, involved electrons and photons in a "clean environment", i.e. in low multiplicity non hadronic interactions.

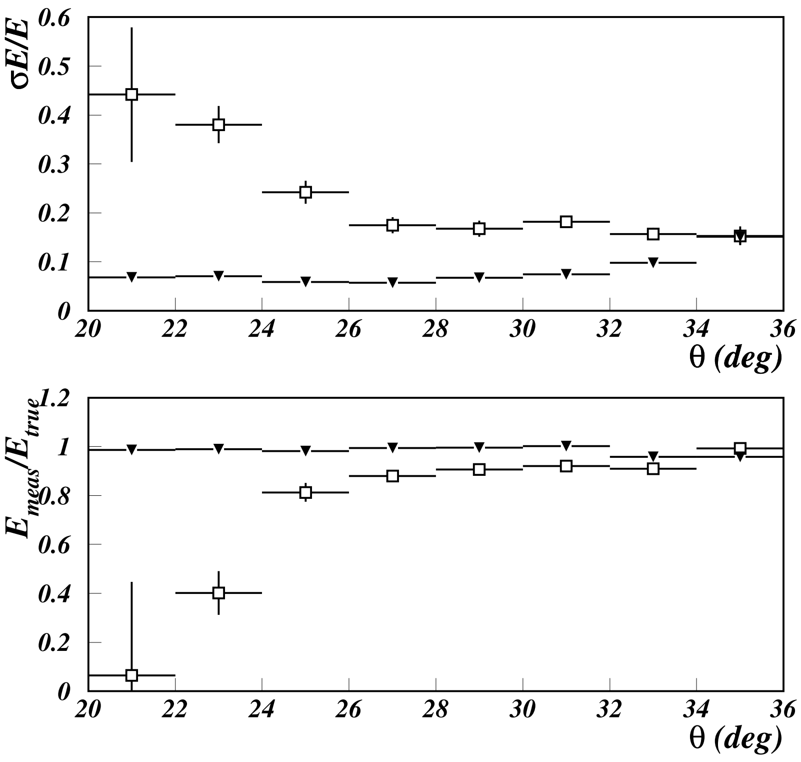

Figure 20: Energy resolution and $E_{particle}/E_{beam}$ obtained using the FEMC (triangle) or the tracking (squares) in the polar range above 20^o for $\sqrt{s} = 91$ GeV

Electro-magnetic clusters inside jets are generated by electrons (produced for example in heavy-flavour quarks decay), photons, π^0s. Compared to isolated electrons and photons coming for example from (semi)leptonic W or Z decays or Bhabhas, they have a lower electro-magnetic energy and an higher hadronic activity around.

Three samples have been considered:

- Bhabhas of type 4 to provide a sample of isolated electro-magnetic showers in a low multiplicity environment;
- high energy photons from hadronic radiative return to the Z to provide a sample of isolated electro-magnetic showers in a high multiplicity environment;
- electrons and photons within jets in hadronic radiative return to the Z to provide a sample of non isolated electro-magnetic showers.

To study the isolation, the ratio R between the energy of the electro-magnetic cluster (E_{clu}) and the total energy (E_{tot}) in a defined region around it has been considered:

$$R = \frac{E_{clu}}{E_{tot}} = \frac{E_{clu}}{E_{clu} + E_{out}} \tag{10}$$

The region around the cluster is defined by:

$$|\theta - \theta_{clu}| \leq 15^o \tag{11}$$

$$|\phi - \phi_{clu}| \leq min\left(15^o, \frac{6^o}{tg(\theta_{clu})}\right) \tag{12}$$

where angles are expressed in degrees.

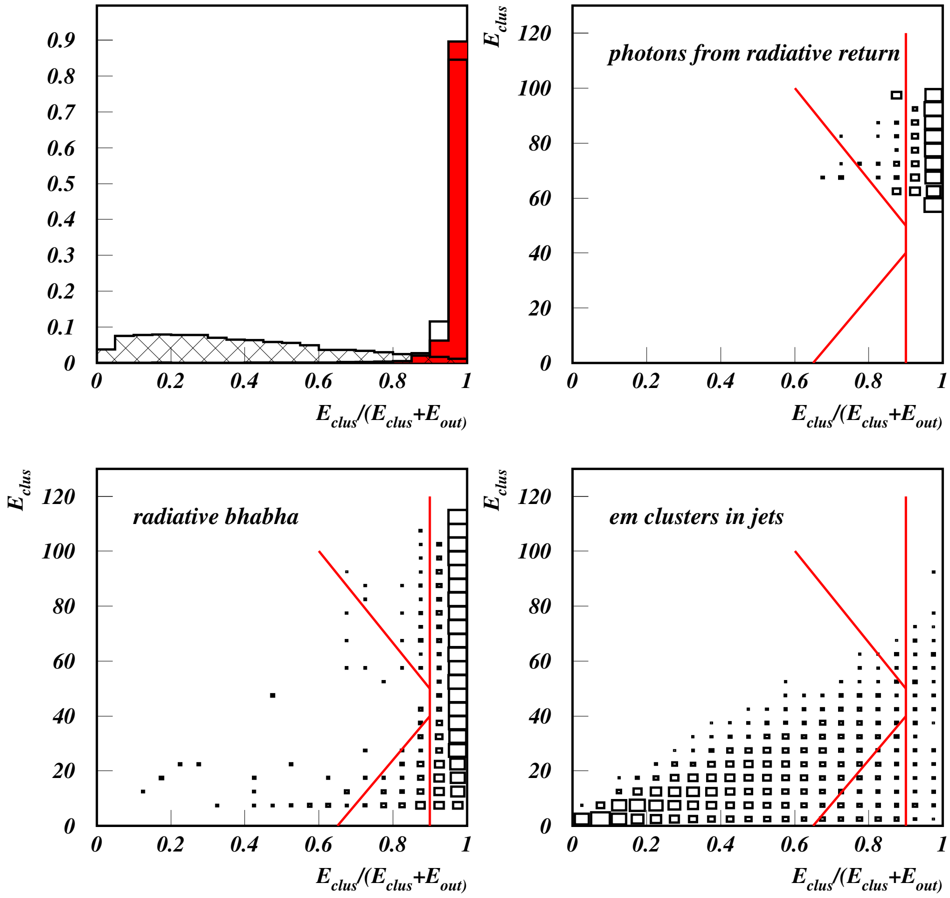

Figure 21: Upper left:R distribution for the Bhabhas (dark), radiative return photons (solid line), photons and electrons in jets(hatched). The other plots show separately for the three samples the dependence of R on the energy of the cluster.

The plot on the upper left corner of fig.21 compare the R distribution for the three samples. The dark histogram refers to Bhabhas, the solid line histogram to radiative return photons, while the hatched one refers to photons and electrons in jets. The other plots show the correlation between R and the energy of the cluster separately for the different type of events. In the scatter plots the entries are normalised in bins of energy, so as to be independent from the energy distribution of the sample. These distributions show that: for very isolated electro-magnetic clusters, of all energies, R is always greater than 90%; for isolated electro-magnetic clusters in an hadronic environment the value of R can be lower, but it is always above 0.6; for electro-magnetic showers inside jets R is in general smaller than 0.6, and can reach higher values only for very energetic clusters. The solid lines on the scatter plots separate regions with different isolation probability. All the clusters are then flagged according to these degree of isolation. No rejection is applied so as to allow the tune of the isolation criteria depending on the topology of the events considered.

4 The REMCLU package

The REMCLU package has been designed to work in the DSTANA frame. At present it does not modify the PV-PA structure of the XSDST, producing instead a list of "electromagnetic clusters" which have a 1 to 1 link with sets of PAs. In the future these clusters might be used to modify the PV-PA structure in a similar way to ELEPHANT/MAMMOTH, but this feature is still not implemented.

The package can be run at the XSDST production level, producing a XSDST bank (link `LQ(LDTOP-33)`) with all the cluster information and the list of the addresses of the PAs used to build each cluster (for more information check the reference [9]).

It can be also rerun on top of the XSDST. Inside the SKELANA frame this is automatically done switching to the appropriate values the flag `IFLECL` [10].

The steering routine `REMCLU` provides all the needed initializations, fills the internal `COMMON` blocks with the needed information, calls the barrel and forward search algorithms and store all the results in a the internal `COMMON PEMCLU` .

The output routine `REMOUT` writes all the information in the format used for the building of the XSDST bank.

If used in the SKELANA frame, the REMCLU output is translated in the SKELANA `COMMON PSCECL` which is an extended copy of the original `PEMCLU` one. This is the suggested way to use the package at present.

Every cluster is made by a primary PA, which is the PA around which the clustering is done, and possibly by a number of secondaries PAs of different kind. Note that since according to the previous definition in the forward algorithm the primary is always an FEMC cluster, it may easily happen that a forward electron has as primary PA a neutral one. Anyway according to the definitions specified below the charged track used for the electron identification can be always unambiguously found.

The `COMMON PSCECL` is filled writing the whole cluster information at the position corresponding to the main PA, and writing for the secondary PAs only the information giving the cluster number and the type of secondary PA. For further details on the use of REMCLU clusters inside SKELANA check reference [10].

The structure of `COMMON PSCECL` is:

```
+KEEP,PSCECL.              Electromagnetic cluster information
*                                       ( EMCL bank (33) )
*
*     NEMCLU                  - Number of elm. clusters             s l
*     LENCLU                  - Length of elm. cluster information
```

```
*     QEMCLU(LENCLU,MTRACK) - Real    array of elm. cluster info
*     KEMCLU(LENCLU,MTRACK) - Integer array of elm. cluster info
*
*     QEMCLU( 1,I) - Best elm. energy estimate of the cluster      s l
*     QEMCLU( 2,I) - Theta angle of the cluster                    s l
*     QEMCLU( 3,I) - Phi   angle of the cluster                    s l
*     QEMCLU( 4,I) - Error on the cluster energy                   s l
*     QEMCLU( 5,I) - Hadronic energy associated to the cluster     s l
*     KEMCLU( 6,I) - Electron/photon identification flag           s l
*                     0 - not identified
*                     1 - tight electron
*                     2 - tight photon
*                    11 - loose electron
*                    22 - loose photon
*                    30 - not identified non isolated (forward)
*                    31 - electron non isolated (forward)
*                    32 - photon non isolated (forward)
*     KEMCLU( 7,I) - 1000*NEMCLU +                                 s l
*                    type of the PA associated to the cluster:
*                    1 - main PA of the cluster
*                    2 - PA with an electromagnetic deposit
*                    3 - PA without an electromagnetic deposit
*     KEMCLU( 8,I) - Number of PA's associated to the cluster      s l
*     KEMCLU( 9,I) - Electric charge of the cluster                s l
*
*     IEMCLU(MTRACK) - List of indices in LVECP of all PA's
*                      associated to elm. clusters in the event    s l
*                      (one-dimentional array)
*
      INTEGER    LENCLU
      PARAMETER (LENCLU =  9)
*
      INTEGER NEMCLU,KEMCLU,IEMCLU
      REAL    QEMCLU(LENCLU,MTRACK)
*
      COMMON /PSCECL/ NEMCLU,IEMCLU(MTRACK)
     +               ,KEMCLU(LENCLU,MTRACK)
      EQUIVALENCE (QEMCLU,KEMCLU)
*
```

Here follows a detailed description:

NEMCLU : counter giving the number of electromagnetic clusters reconstructed in the event by the package.

QEMCLU(1,I) : best estimate of the energy of the electromagnetic cluster. This is the electron/photon energy to be used in the analyses.

`QEMCLU( 2,I)` : polar angle θ of the cluster.

`QEMCLU( 3,I)` : azimuthal angle ϕ of the cluster. Note that both the polar and the azimuthal angle are computed following the standard DST main module convention, i.e. they are referred to the DELANA primary vertex.

`QEMCLU( 4,I)` : estimate of the error on the cluster energy.

`QEMCLU( 5,I)` : hadronic calorimeter energy falling in a predefined cone behind cluster (see the previous sections for further details). It is the energy used for the isolation definition and the hadron veto. It is not included in the best energy definition (which is only of electromagnetic origin).

`KEMCLU( 6,I)` : Electron/photon identification flag. In the barrel part the first 5 values are allowed:

- 0 : not identified;
- 1 : tight electron: below 30 GeV means PXPHOT code 4 or 5, above it requires that the hadron calorimeter energy `QEMCLU( 5,I)` be less than 10% of the electromagnetic one (25% close to the HPC cracks);
- 2 : tight photon: below 25 GeV good PXPHOT HPC photons not failing profile cuts, above if not tagged or tagged as π^0 basic requests on the number of HPC rows, consecutive rows and first row hit position;
- 11 : loose electron: below 30 GeV means PXPHOT code 3, above the candidates failing the above cuts on the ratio hadronic/electromagnetic energy.
- 22 : loose photon: below 25 GeV PXPHOT photons failing the transverse profile cuts but close to HPC z cracks, above PXPHOT photons failing either the transverse of the longitudinal or both profile cuts close the HPC z cracks.

In the forward part all the values are possible, distinguishing between isolated and not isolated clusters; the isolation criteria is based on the hadronic/electromagnetic energy ratio in a cone around the cluster:

- 0 : isolated not identified;
- 1 : isolated tight electron: one and only one associated VD-VFT track, not more than one track with ID+TPC;
- 2 : isolated tight photon: no track with VD-VFT, TPC+ID or if below 20^o ID+FCH or if below 15^o FCH. Below 11^o no tight photon identification is provided: all clusters which do not fulfill the tight electron criteria are are classified as unknown. Note that also tight photon can have tracks associated;
- 11 : isolated loose electron: no track in VD-VFT but one and only one associated track TPC+ID or, if the polar angle is below 20^o, a ID+FCH one;
- 22 : isolated loose photon: two tracks associated with TPC+ID or ID+FCH but no VD-VFT hits, or no track in VD-VFT but a track with TPC+ID or if below 20^o ID+FCH;
- 30 : not identified not isolated;

31 : non isolated electron;

32 : non isolated photon.

It should be noted that the non isolated tags in the forward region have to be treated with great care, since the isolation can depend significantly on the topology under study.

`KEMCLU( 7,I)` : flag to associate a PA to a cluster and to characterise its own role in the cluster; its value is $1000 \times N_{cl} + 10 \times I_{vtx} + I_{sec}$ where:

N_{cl} : sequential number of the cluster in the event which the PA `I` is associated to;

I_{vtx} : 0 if the PA is hanging on the primary or dummy vertex, 1 if it is exiting a secondary vertex produced by ELEPHANT/MAMMOTH;

I_{sec} : kind of PA in the cluster:

1 : main PA of the cluster;

2 : secondary PA with electromagnetic energy;

3 : secondary PA without electromagnetic energy (forward);

4 : secondary PA without electromagnetic energy (barrel).

Note that the secondary PAs without electromagnetic energy definition has a quite different meaning in the barrel and in the forward search: in the barrel they are used only to evaluate the isolation, and are not part of the cluster, i.e. they have to be used in the analysis (if accepted by the user track selection). In the forward search they are integral part of the cluster (for instance a VD-VFT only track has no electromagnetic energy associated by definition, but can easily be the incoming electron candidate track associated by REMCLU with a neutral PA in the FEMC);

`KEMCLU( 8,I)` : number of PAs associated to the cluster;

`KEMCLU( 9,I)` : electric charge according to the SKELANA convention (0 neutral, +1 positive, -1 negative, 3 unknown).

The array `IEMCLU(I)` gives the cluster sequential number corresponding to the PA placed in the `I`-th position in the SKELANA arrays `LVECP,VECP, ...`

5 Acknowledgements

We would like to thank P. Checchia, M. Elsing, V. Hedberg, S. Marti and A. Ouraou for the useful discussions, suggestions and cross checks that have helped us in the development of the algorithms. We also thank T. Spassoff for the preparation of the DST interface of REMCLU.

References

[1] C. Kreuter, M. Feindt, O. Podobrin, *ELEPHANT Reference Manual*, DELPHI 96-82 PROG 217 (1996);
see also references in `http://home.cern.ch/ pubxx/tasks/elephant/www/Welcome.html`

[2] M. Elsing, *Summary of the updates in the DELPHI forward tracking to include the VFT*, DELPHI 98-5 PROG 227 TRACK 91 (1998)

[3] DELPHI Collaboration, *DELPHI Data Analysis Program (DELANA) User's Guide*, DELPHI 89-44 PROG 137 (1989)

[4] V. Hedberg,
http://delphiwww.cern.ch/ pubxx/delwww/tasks/lep200/searches/teama/www/forward/

[5] P. Checchia, A. Lopez, M. Zito, *Electron detection and reconstruction*, DELPHI 89-73 PHYS 54 PROG 143 (1989)

[6] M. Paganoni, S. Gumenyuk, F. Terranova, V. Obraztsov, M. Bigi, I. Gouz, E. Migliore, *Energy and position reconstruction in the DELPHI Small Angle Tile Calorimeter*, DELPHI 97-8 PHYS 666 (1997)

[7] P. Checchia and P. Ronchese, *A study of photon conversion probability in* $e^+e^- \rightarrow \gamma\gamma$ *events*, DELPHI 96-130 PHYS 633 (1996)

[8] M. Verlato, *La ricerca di nuova fisica a LEP mediante lo studio di eventi con soli fotoni nello stato finale*, Ph.D. Thesis, Università degli Studi di Padova (1997)

[9] T. Spassoff, *DELPHI Extended ShortDST Content*, DELPHI 97-147 PROG-222 Rev. 2 (2000)

[10] F. Cossutti et al, *Improvements to SKELANA for Version 2.0*, DELPHI 99-175 PROG 239 (1999)

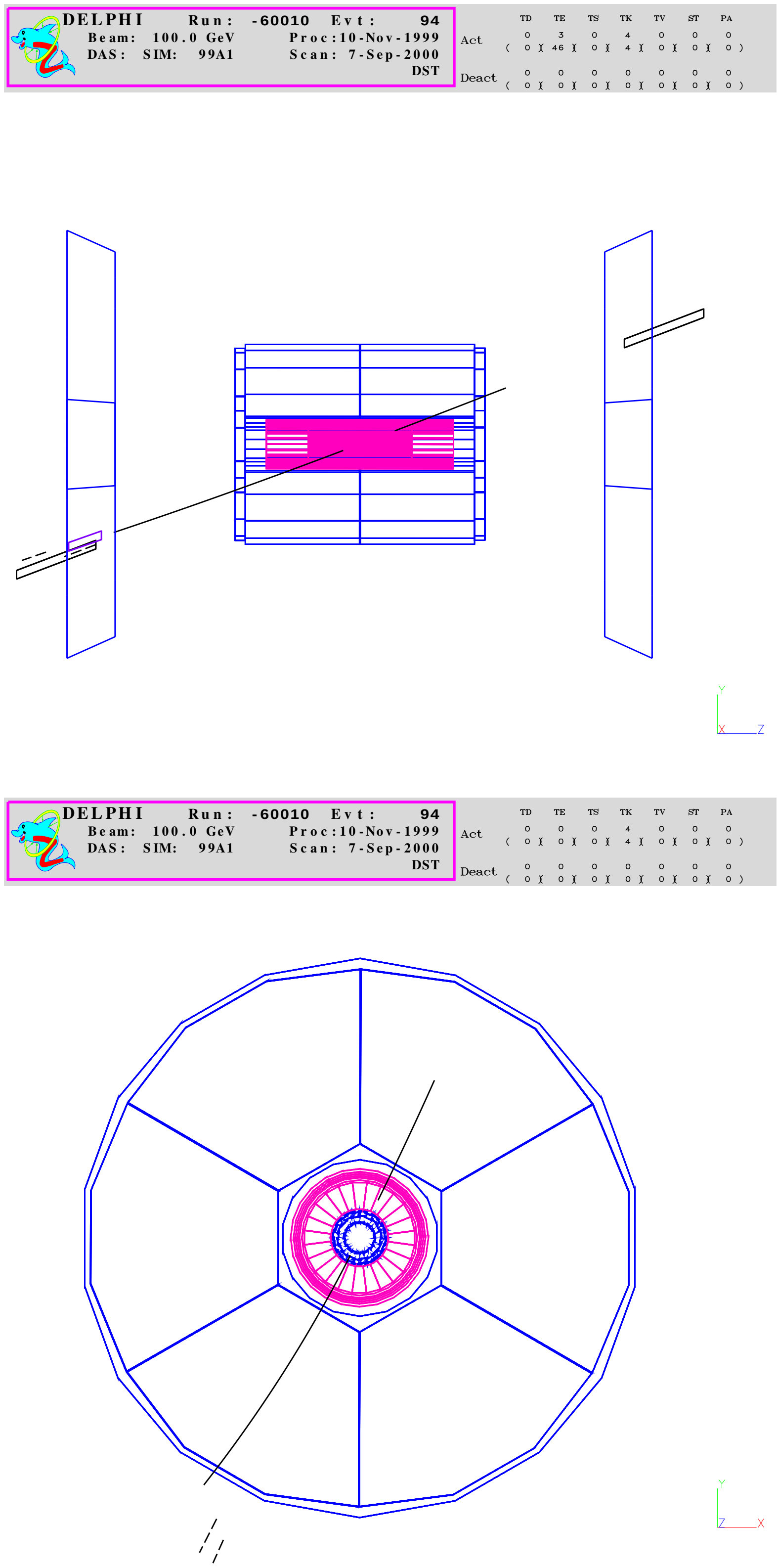

Figure 22: The display shows in the (z,y) -top- and (x,y) -bottom- views a simulated Bhabha event: one of the electrons is tagged as tight (left) while the other (right) as loose. The loose electron is identified thorugh a clean TPC+ID track (but with no VD information)

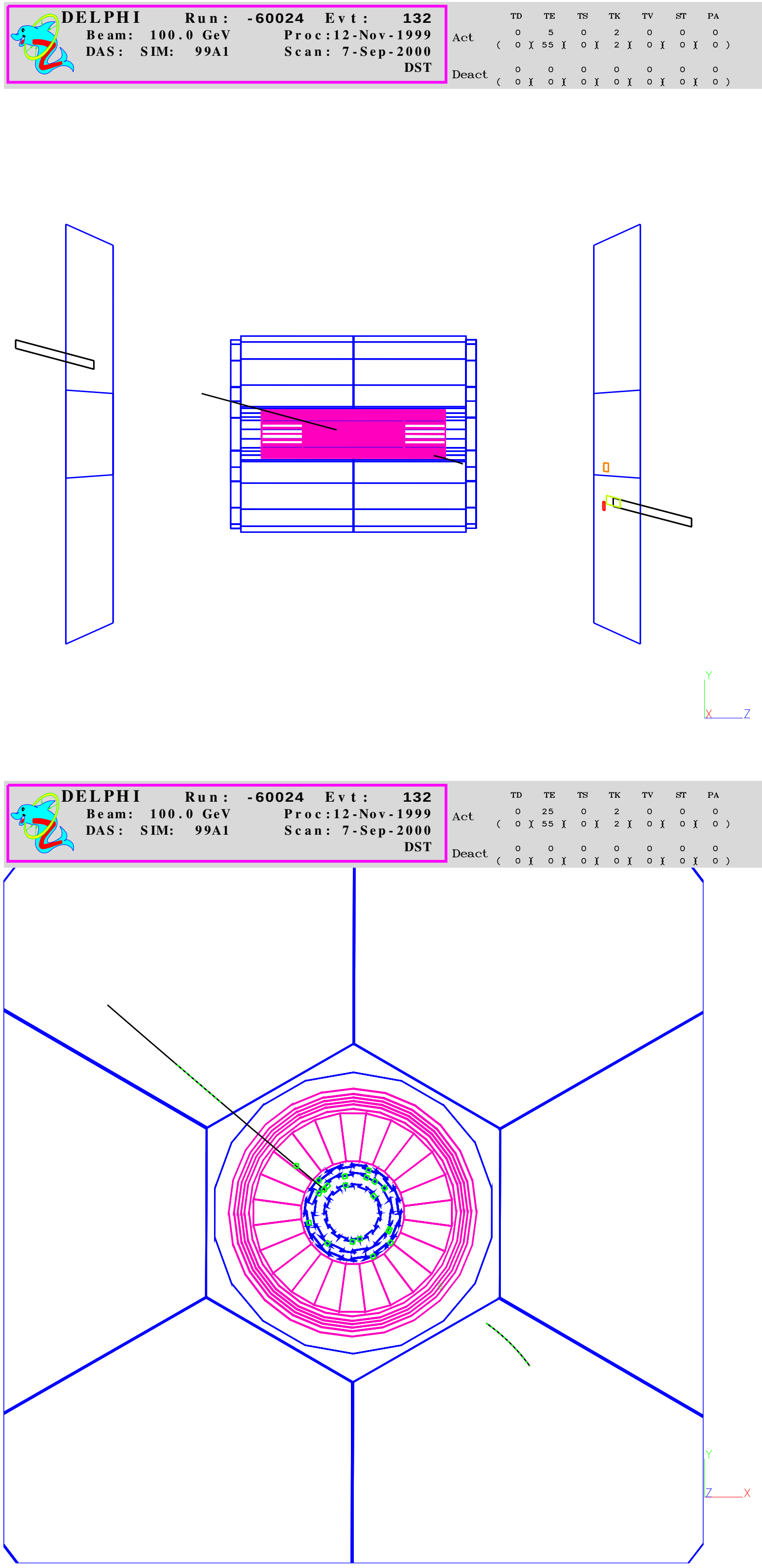

Figure 23: The display shows in the (z,y) -top- and (x,y) -bottom- views a simulated Bhabha event: one of the electrons is tagged as tight electron (left) while the other (right) as tight photon. This electron is at $\theta = 23^o$ but has no charged track around with VD or ID hits, only a very soft tracks in the TPC.

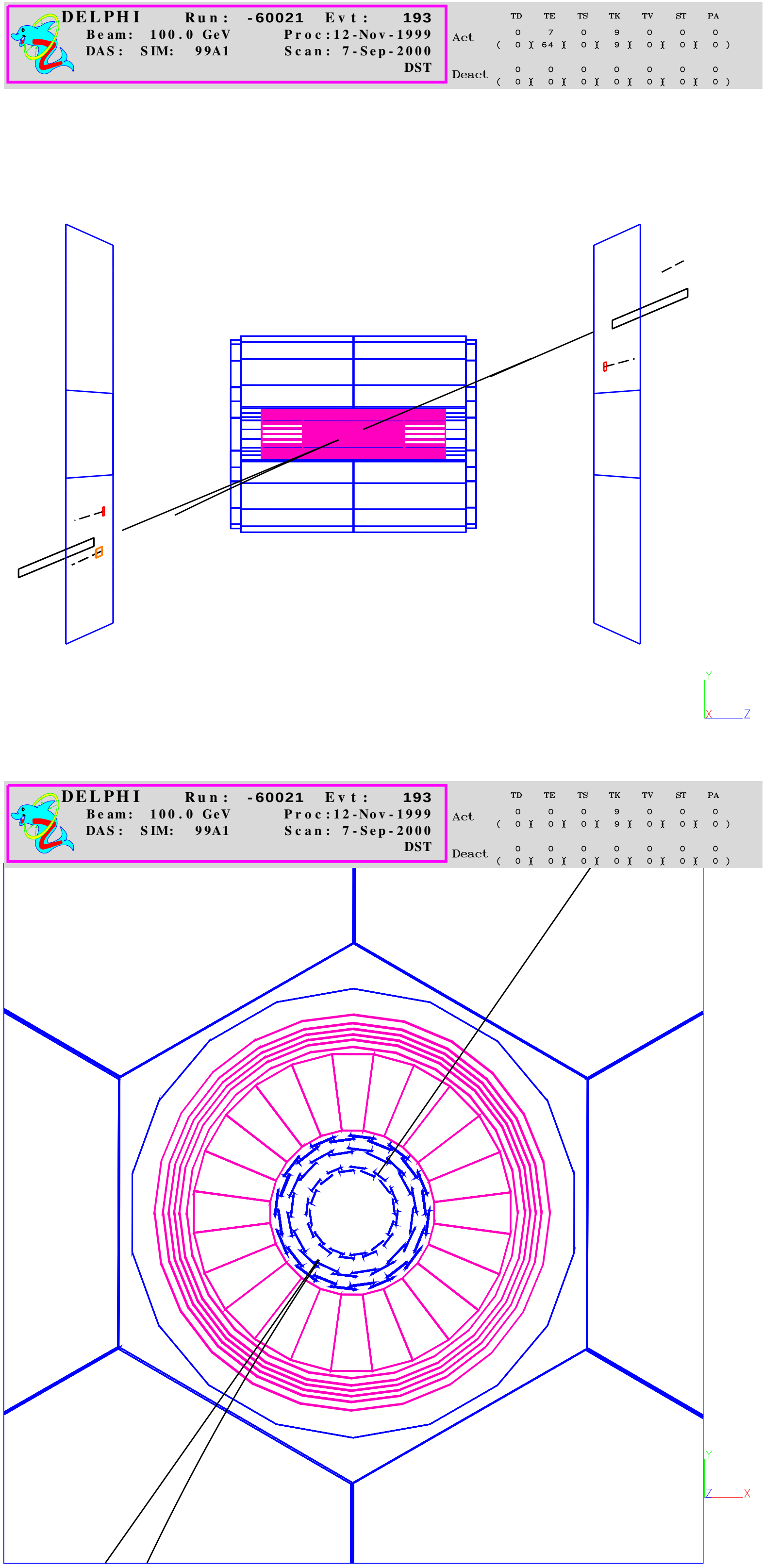

Figure 24: The display shows in the (z,y) -top- and (x,y) -bottom- views a simulated Bhabha event: one of the electrons is tagged as tigh (right) while the other as unknown because it has two associated tracks starting from the VD.

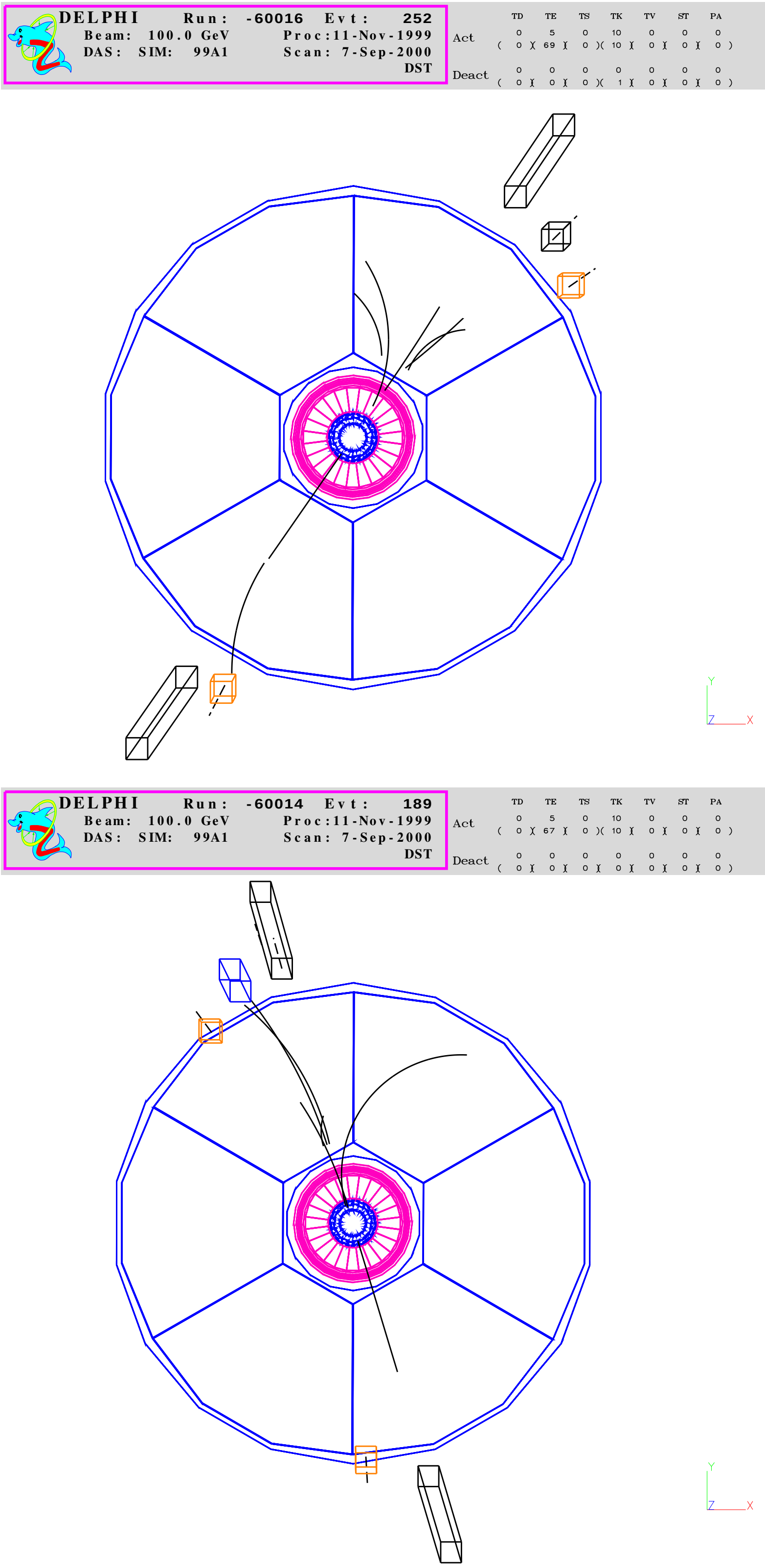

Figure 25: The display shows in the (x,y) view two simulated Bhabha events: in both one of the electrons is tagged as tight (top-left and down-right) while the other as unknown. These are examples of electrons developing an electromagnetic shower already in the VD (bottom) or ID (top)

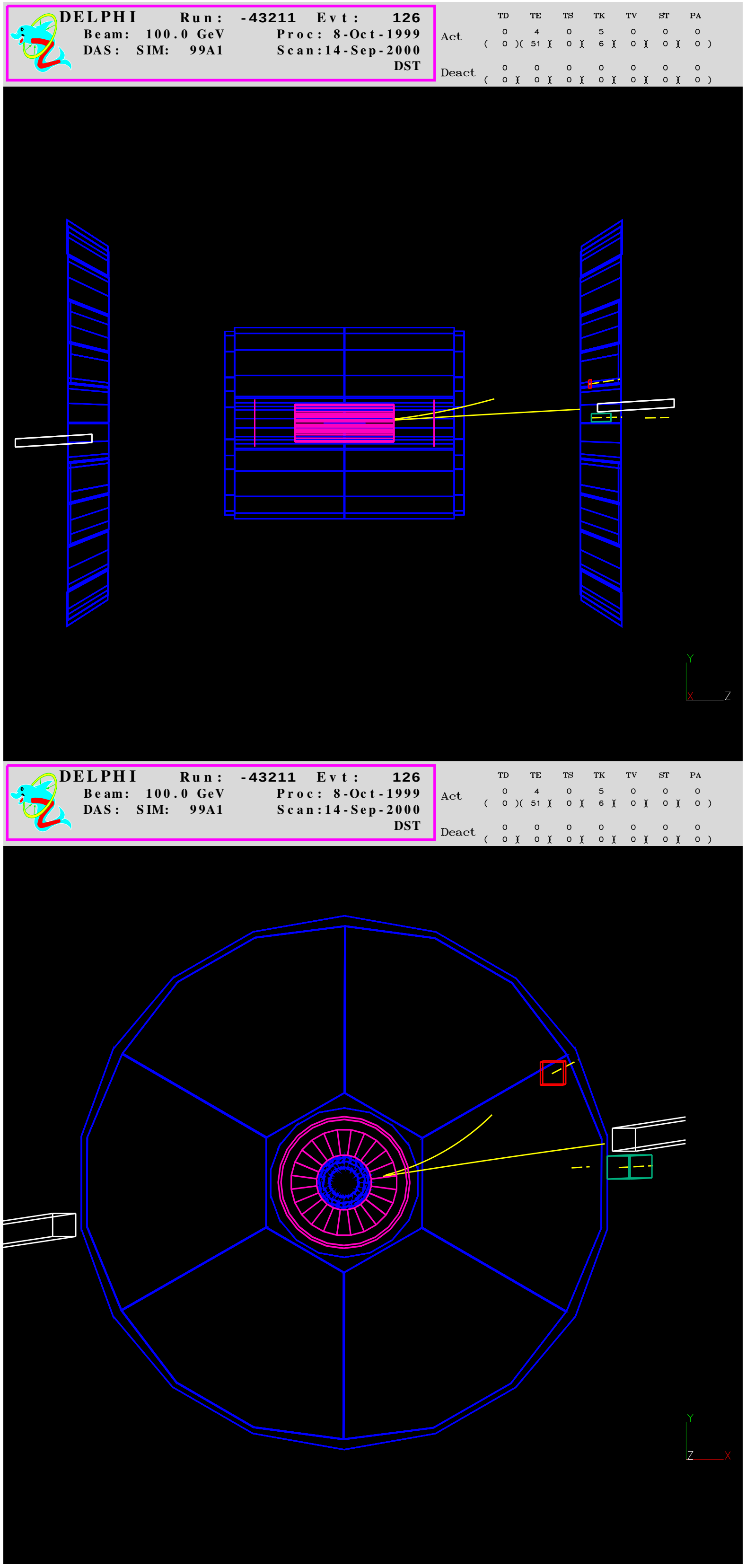

Figure 26: The display show in the (z,y) -top- and (x,y) -bottom- view a simulated $\gamma\gamma$ (QED) event: one of the photons is tagged as tight (left) while the other as loose. The loose photon indeed converts before the FEMC and two clean tracks with ID+TPC are visible in the detector.

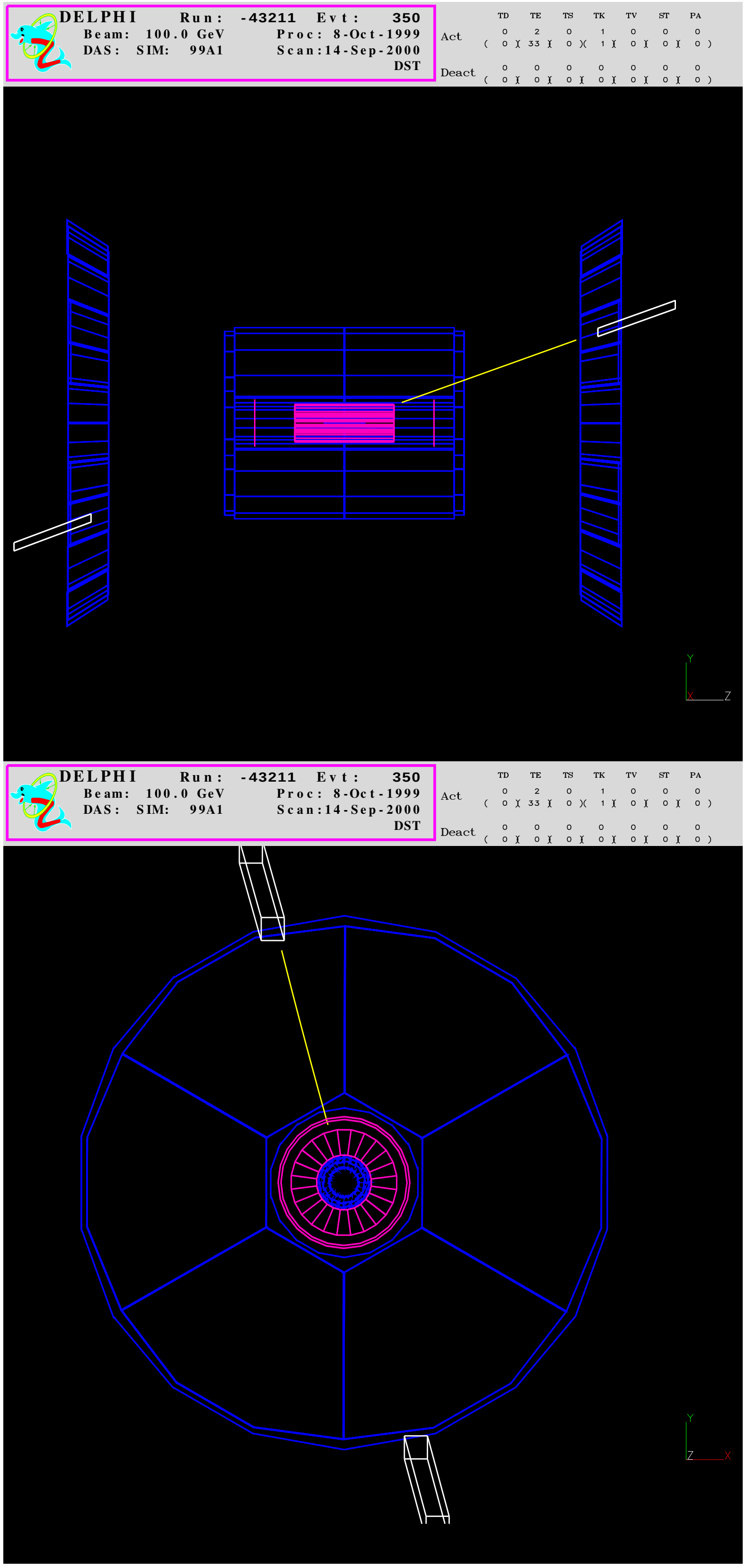

Figure 27: The display show in the (z,y) -top- and (x,y) -bottom- view a simulated $\gamma\gamma$ (QED) event: one of the photons is tagged as tight photon(left) while the other as loose electron. The photon tagged as loose eletron converts before the ID but only one clean track is reconstructed with ID+TPC hits.

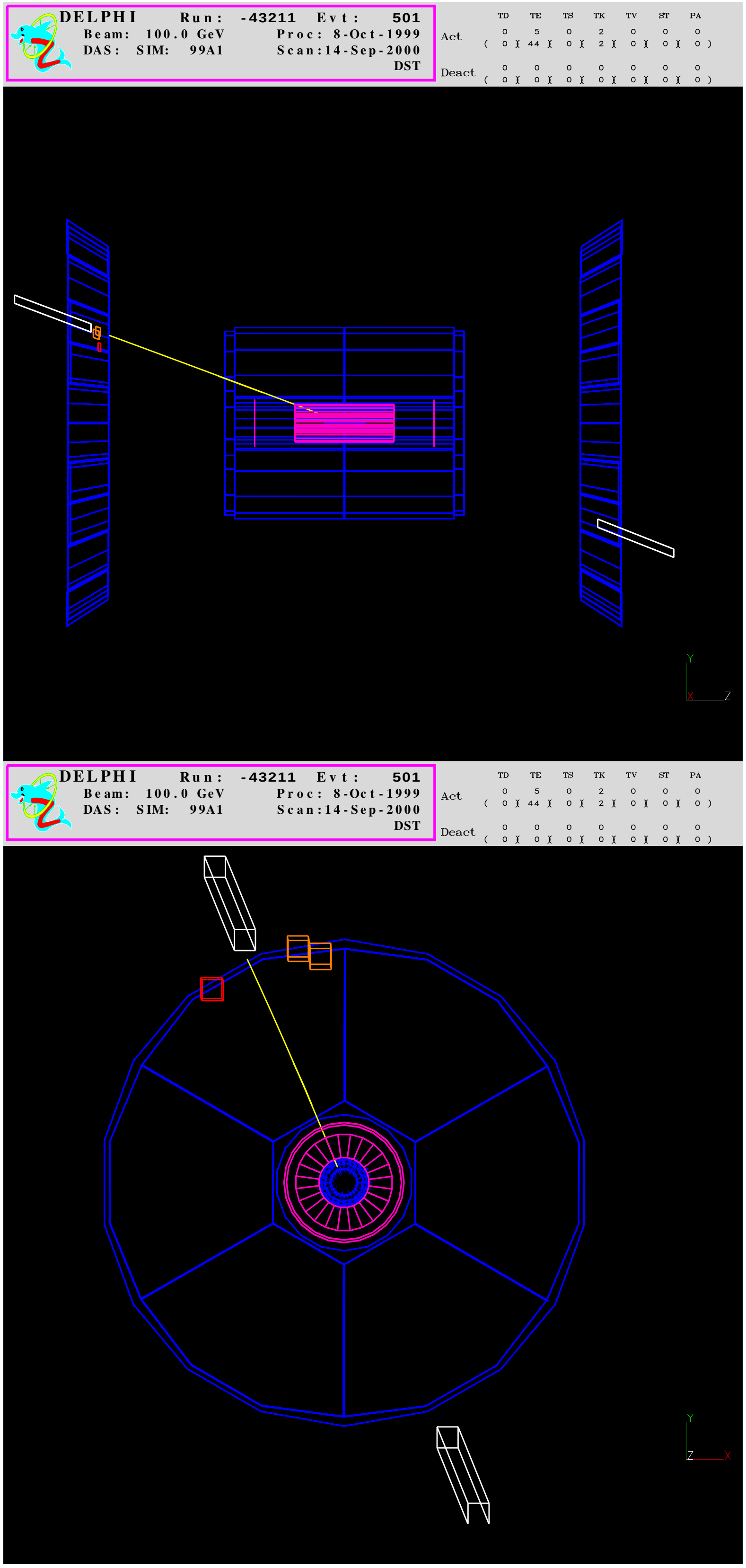

Figure 28: The display show in the (z,y) -left- and (x,y) -right- view a simulated $\gamma\gamma$ (QED) event: one of the photons is tagged as tight photon(left) while the other as tight electron. The photon tagged as tight eletron converts in the VD but only one clean track is reconstructed.